ADVANCED MATERIALS
www.advmat.de

Self-Powered Active Sensing Based on Triboelectric Generators

*Gaurav Khandelwal and Ravinder Dahiya**

The demand for portable and wearable chemical or biosensors and their expeditious development in recent years has created a scientific challenge in terms of their continuous powering. As a result, mechanical energy harvesters such as piezoelectric and triboelectric generators (TEGs) have been explored recently either as sensors or harvesters to store charge in small, but long-life, energy-storage devices to power the sensors. The use of energy harvesters as sensors is particularly interesting, as with such multifunctional operations it is possible to reduce the number devices needed in a system, which also helps overcome the integration complexities. In this regard, TEGs are promising, particularly for energy autonomous chemical and biological sensors, as they can be developed with a wide variety of materials, and their mechanical energy to electricity conversion can be modulated by various analytes. This review focuses on this interesting dimension of TEGs and presents various self-powered active chemical and biological sensors. A brief discussion about the development of TEG-based physical, magnetic, and optical sensors is also included. The influence of environmental factors, various figures of merit, and the significance of TEG design are explained in context with the active sensing. Finally, the key applications, challenges, and future perspective of chemical and biological detection via TEGs are discussed with a view to drive further advances in the field of self-powered sensors.

1. Introduction

Sensors are vital for digital transformation that is currently taking place through rapidly evolving concepts such as industry 4.0, Internet of Things (IoT), smart homes and buildings, smart cities, smart transportation, and digital health etc.[1] They make critical components of the enabling technologies (e.g., wearable systems, robotics, augmented reality (AR)/virtual reality (VR), and interactive systems etc.[2] for above concepts. These technological tools require a large number of different types of sensors for real-time monitoring of the parameters of interest, with the aim of increasing efficiency or productivity, enabling predictive actions (e.g., maintenance, monitoring potential hotspots for spread of diseases) and optimizing supply chain and asset traceability while developing a safer and more secure environment. Accordingly, numerous physical, chemical, and biosensors based on different working mechanisms and transducer materials have been reported.[3–6] Most of these sensors require continuous operation, for which reliable power source is critical.

The widely used power source is the batteries that are often bulky, have a limited lifetime, and are difficult to recycle because of toxic chemicals.[7] As a result, they compromise the sensors portability and, in certain cases, also require a complex and costly process to replace after they run out. Coin cells are other alternatives that are now heavily commoditized and usually present a low-cost solution for powering standalone, lightweight, portable, and miniaturized sensors. However, they still require replacement at regular intervals. A self-reliant and sustainable way of powering the sensors to acquire data and send them wirelessly to a data hub, would be ideal. One solution is to combine a small, long-life, energy-storage devices (e.g., a supercapacitor or a rechargeable solid-state battery) with an energy harvester or wireless powering device.[8] There are many ways of harvesting energy from the environment, from solar energy using photovoltaic panels, or heat using thermal electric generators and vibration with piezoelectric and triboelectric generators (TEGs).[9] Herein, we use the term triboelectric generator (TEG), which also covers the triboelectric nanogenerators (TENGs). If the energy budget is balanced correctly, these two components, i.e., energy storage device and the energy harvester, do not need to be large to work for a long time. The availability of ultralow-power electronics and the constantly improving efficiency of energy harvesting devices (e.g., high-efficiency indoor solar cells can provide at least 20 mW cm^{-2} and the TEGs can provide up to 50 mW cm^{-2}) also support such solutions.[9a,10] Further, the sensors and power management integrated components are becoming increasingly less power hungry.[7b] However, this approach

G. Khandelwal, R. Dahiya
Bendable Electronics and Sensing Technologies (BEST) Group
James Watt South Building
School of Engineering
University of Glasgow
Glasgow G12 8QQ, UK
E-mail: ravinder.dahiya@glasgow.ac.uk

The ORCID identification number(s) for the author(s) of this article can be found under https://doi.org/10.1002/adma.202200724.

DOI: 10.1002/adma.202200724

still requires separate energy and sensors devices and need for large number of such devices in application such as wearable systems may lead to integration challenges. The solution lies in active or self-powered sensors, i.e., the sensors that do not require external power for transduction. In other words, the energy devices themselves can be used as sensors. As an example, we recently demonstrated the use of supercapacitor, solar cell, and TEG devices as a strain sensor, touch sensor, and pressure sensor respectively.[8b,11]

For applications having moving parts, mechanical energy harvesters such as piezoelectric nanogenerators (PENGs) and TEGs could provide attractive solution as self-powered sensors.[12] TEGs have an edge over PENGs due to their high output, wide range of device design, and the materials. PENGs have a material restriction, i.e., only materials that exhibit piezoelectricity can be used. Furthermore, poling is required to align the dipoles for increasing the device output.[5a] Further, TEGs can be developed from a wide range of triboelectric materials, which includes natural materials, metals, metal oxides, 2D materials, conventional polymers, crystalline coordination polymers, ferroelectric materials, and textiles.[5a,13] The output of the TEGs can be tuned by creating surface nano/microstructures, ion implantation and chemical functionalization or modifications,[14] thus allowing their use as self-powered physical, chemical and biosensors[6k,15,16] As a result, the scientific community is actively exploring TEGs as to address the issues associated with powering of sensors.

The supremacy of TEGs combined with the advances in nanotechnology can bring revolutionary advances in the self-powered sensors, device designs and portability. Therefore, this review article focuses on TEG-based active or self-powered sensors and presents up-to-date advancements in the area. The discussion herein complements previous review articles where advances related to physical, chemical and biosensors have been presented separately.[6k,15,17] Our primary focus here is on the TEG as enthralling technology for the active chemical and biosensors. The paper starts with brief description of the major historical milestones in the field of mechanical energy harvesting, leading up to TEG-based physical, magnetic and optical active sensors. **Figure 1** summarizes the application of TEG as an active physical, magnetic, optical, chemical and biosensor. Section 2 discusses the historical evolution of TEG and the trends. The TEG basic working mechanism, figure of merits (FOM), and comparison with conventional sensors are discussed in Section 3. The first three, i.e., physical, magnetic, and optical sensors are described in Section 4. The self-powered chemical and biosensors and their pros and cons are explained in Section 5 and Section 6 respectively. This is followed by a description of the major applications of self-powered chemical and biosensors in Section 7. Finally, the challenges and opportunities in the field are discussed is Section 8 along with future research directions.

2. Mechanical Energy Harvesting and TEG-Based Sensors—Historical Evolution

Figure 2A shows major historical milestones related to mechanical energy harvesters. Their history dates back to 1831, when the electromagnetic generator (EMG) was developed by the Faraday.[34d,35] The EMG has been recently used with TEGs to develop a hybrid generator for oil spill detection, wireless sensor, and seismic detection.[35–36] Maxwell's equation, proposed in 1861, unifies the electromagnetism and Maxwell's displacement current equation was used to drive theoretical calculation of TEGs.[34d,37] In early 2000s, PENG-based energy harvesters and sensors started to appear for application such as wearable systems and tyre pressure monitoring.[34a] More recently the TEG has been dominating over other energy-harvesting approaches due to the advantages mentioned in previous section.[12] This dominance is also evident from Figure 2B, which shows the growth in the number of publications on topics related to TEGs, PENGs, and TEG- and PENG-based sensors from the time they were first reported.

3. Triboelectric Generator Working Principle, Device Modes, and Sensing Mechanism

Contact electrification or triboelectric effect is the process where a material surface gets electrically charged when it comes in proximity or in contact with the other material. Electrostatic induction is the redistribution of the electrical charges due to the influence of nearby charges. Contact electrification dates back to ≈2600 years. In 1762, Johan Carl Wilcke invented electrophorus which was a capacitive electrostatic generator. Electrophorus uses electrostatic induction to produce electrostatic charges. Briefly, electrophorus comprised a metal plate and a dielectric plate, where dielectric plate was initially charged via the triboelectric effect using cloth or a fur. The metal plate when placed on the dielectric, leads to charge separation in the metal plate due to the electrostatic field of the charged dielectric. Basically, electrophorus separates the negative and positive charges in the plate and the charge on the top face can be drained by grounding. As a result, the metal plate is left with either a negative or a positive charge.[38] James Wimshurst invented an electrostatic generator (Wimshurst generator) that can produce high DC voltages using the electrostatic induction.[39] Later, Robert J. Van de Graaff invented an electrostatic generator (Van de Graaff generator) to produce high-voltage DC. The Van de Graaff generator uses triboelectric effect to develop charges unlike Wimshurst machine.[40] While TEG is a mechanical energy harvester driven by the coupling of contact electrification and electrostatic induction. Contact electrification or triboelectrification is ubiquitous and can happen between almost all materials. The first flexible TEG was developed in 2012.[12] Generally, when two distinct materials meet each other, they develop equal and opposite charges depending on their surface properties. The opposite charges developed on the back electrodes via electrostatic induction give rise to a potential difference during the periodic motion. The process will allow the flow of electrons between the electrodes to produce an AC output. The TEG can be treated as a device whose capacitance varies. The TEG produces electricity by physical contact which can be a solid–solid contact or solid–liquid contact. In solid–solid contact, electron transfer is the source of contact electrification. When two solid comes close to each other, they form an overlapped cloud of electrons, leading

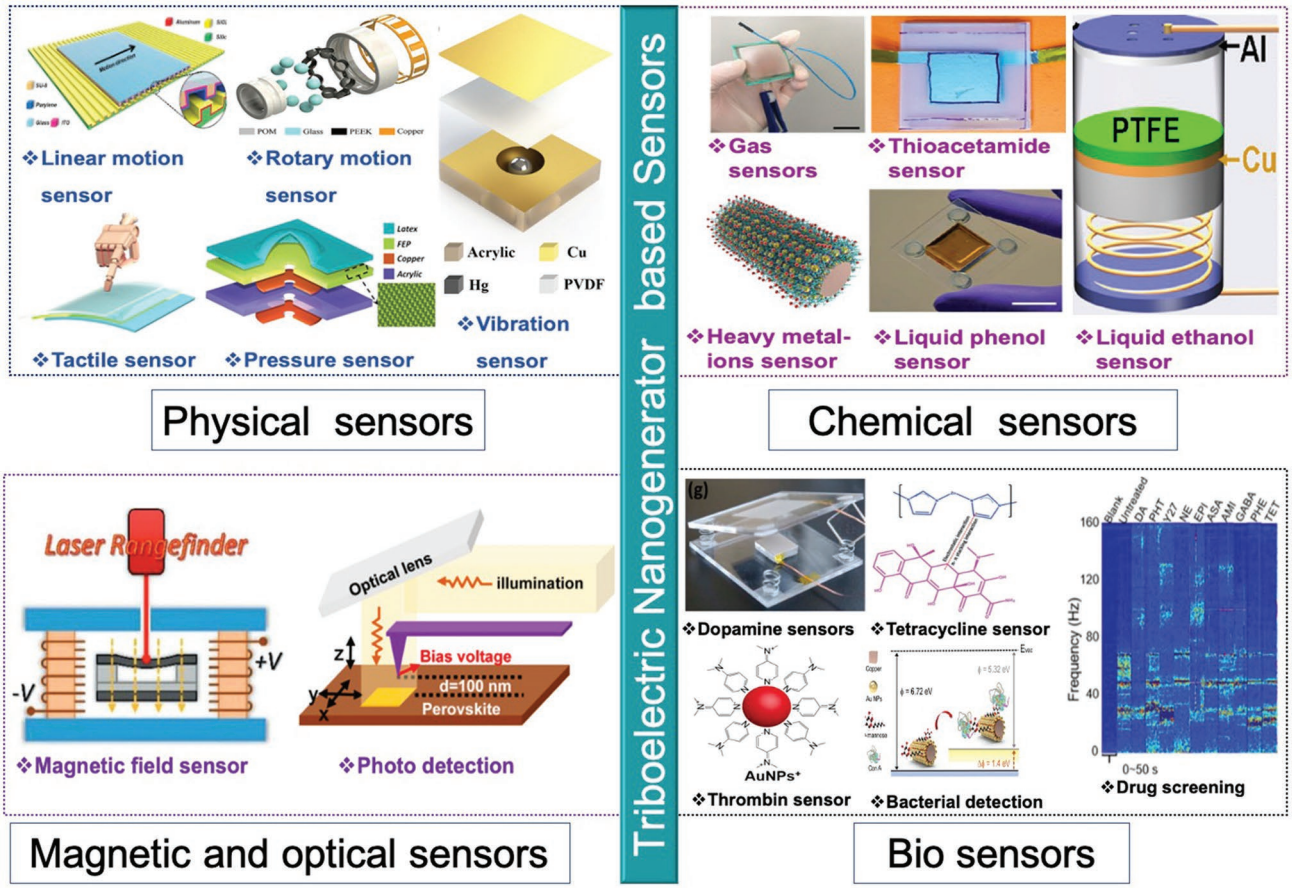

Figure 1. TEG-based active sensors. Linear motion sensor: Reproduced with permission.[18] Copyright 2013, Wiley-VCH. Rotary motion sensor: Reproduced with permission.[19] Copyright 2019, Elsevier. Vibration sensor: Reproduced with permission.[20] Copyright 2017, American Chemical Society. Tactile sensor: Reproduced with permission.[21] Copyright 2017, American Chemical Society. Pressure sensor: Reproduced with permission.[22] Copyright 2014, Wiley-VCH. Gas sensors: Reproduced with permission.[23] Copyright 2020, American Chemical Society. Thioacetamide sensor: Reproduced with permission.[24] Copyright 2021, American Chemical Society. Heavy-metal-ion sensor: Reproduced under the terms of the CC-BY Creative Commons Attribution 4.0 International License (https://creativecommons.org/licenses/by/4.0/).[25] Copyright 2020, The Authors, published on behalf of The Electrochemical Society by IOP Publishing Ltd. Liquid phenol sensor: Reproduced with permission.[26] Copyright 2015, Royal Society of Chemistry. Liquid ethanol sensor: Reproduced with permission.[27] Copyright 2013, Elsevier. Magnetic field sensor: Reproduced with permission.[28] Copyright 2018, Royal Society of Chemistry. Photodetection: Reproduced with permission.[29]Copyright 2015, American Chemical Society. Dopamine sensors: Reproduced with permission.[30] Copyright 2015, American Chemical Society. Tetracycline sensor: Reproduced with permission.[5b] Copyright 2019, John Wiley and Sons. Thrombin sensor: Reproduced with permission.[31] Copyright 2016, Elsevier. Bacterial detection: Reproduced with permission.[32] Copyright 2021, Elsevier. Drug screening: Reproduced with permission.[33] Copyright 2020, American Chemical Society.

to the electron transfer. When two solid separates, the electron transfer leads to the formation of charged surfaces by contact electrification.[41] The contact electrification at the solid–liquid interface is a complex phenomenon which involves the coupling of numerous physiochemical effects. The conventional electric double layer (EDL) concept at the solid–liquid interface was replaced by total density of states (TDOS) which consider more complex factors to reflect the variation in the charge density.[42] The solid–liquid TEG with interfacial engineering is advantageous in liquid energy harvesting.[42–43] So far, TEGs have been developed using four operating modes (**Figure 3**)—the vertical contact-separation (C-S), lateral sliding (LS), single electrode (SE), and freestanding layer triboelectric (FT).[12,44] While the basic working mechanism of all four modes is the same, they differ in terms of design, relative motion, applied force and performance.

The TEG-based chemical sensor and biosensor are based on the interaction of the analyte with the active layer, which influences the TEG output. Most of the reported TEG-based chemical and biosensors have utilized C-S mode because of simple design, and operational stability.[44b] Additionally, the C-S mode allows controlled experiments for the sensing measurements. In LS mode the triboelectric effect can be high, but there is greater wear and tear. The performance of various modes of TEGs is compared using performance related figures of merit (FOM_P), which cover structural (FOM_S) and material (FOM_M) aspects. The cycles for maximized energy output (CMEO) were derived from the V-Q plot for the maximum energy generated by the TEG. The FOM_S for different TEG modes were simulated using the finite element method (FEM) and analytical formula. FOM_M depends on the surface charge density (σ), which is related to the material. FOM_M relates to the square of

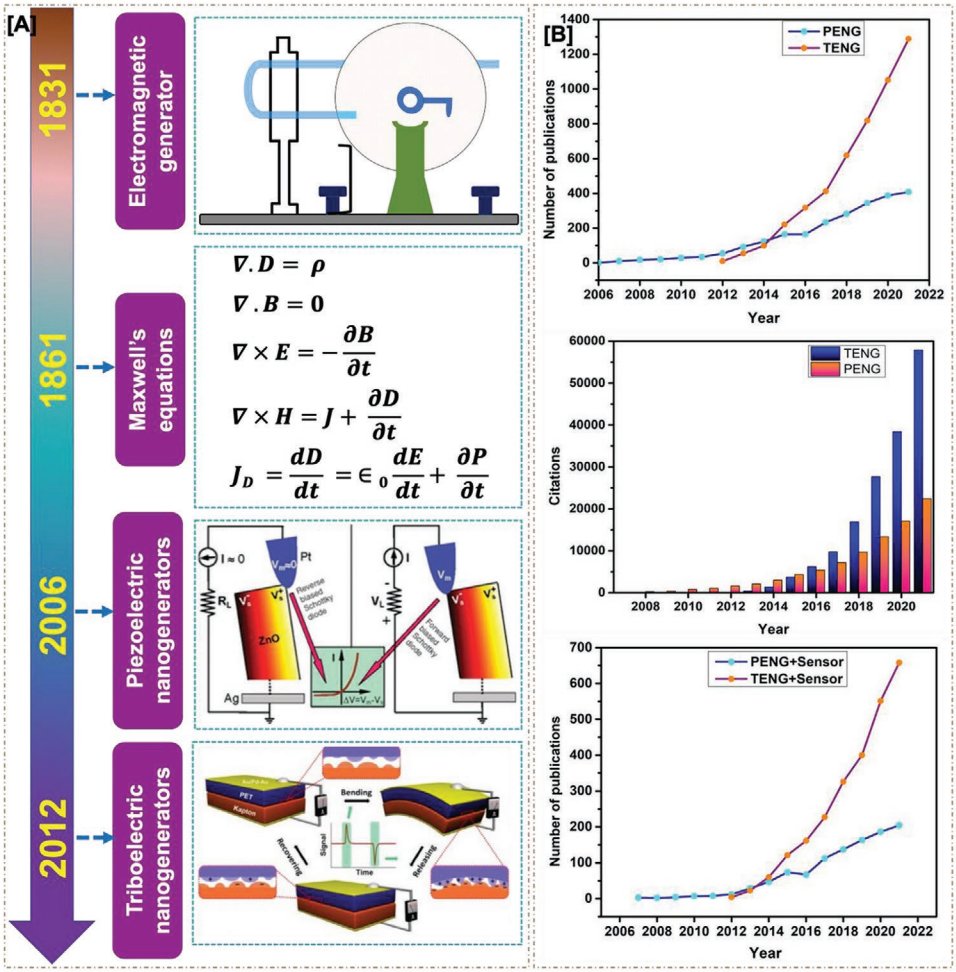

Figure 2. A) Major milestones in the field of mechanical energy harvesting.[12,34] B) Trends showing the number of publications and citations related to TEGs, PENGs, and TEG- or PENG-based sensors. The data was obtained from Web of Science using the keywords "piezoelectric nanogenerator" for PENG; "triboelectric nanogenerator" OR "triboelectric generator" for TEG; "piezoelectric nanogenerator" AND "sensor" for PENG + Sensor and "triboelectric nanogenerator" OR "triboelectric generator" AND "sensor" for TEG + Sensor. All the searches were performed on 12 March 2022. Image for piezoelectric nanogenerators (2006): Reproduced with permission.[34a] Copyright 2006, American Association for the Advancement of Science. Image for triboelectric generators (2012): Reproduced with permission.[12] Copyrigh 2012, Elsevier.

the materials surface charge density. The FOM_M was checked by measuring the σ with liquid metal as a contact. The trend FOM_S follows is: contact FT mode (CFT) > CS > sliding FT (SFT) > LS > single electrode contact mode (SEC).[45] Although the FT mode TEGs offer the highest FOM_P they have a complex structure and fabrication process.[46] The high-output TEG can be fabricated by carefully selecting the materials from the triboelectric series. The general rule of thumb is to select the materials that lie far apart in the triboelectric series to fabricate high-output TEGs. The output of TEGs can also be enhanced by tailoring the surface properties and controlling environment factors such as humidity, temperature, force, and frequency.[10,16,47] To a certain extent, the effect of humidity and temperature can be controlled by the careful selection of material and suitable packaging.[48]

TEGs offer several advantages over the conventional sensors based on the amperometric and potentiometric detection methods. The selectivity of the electrochemical sensors is improved with the functionalization, hybrid materials, use of antibodies and enzymes. The conventional sensors require external power source for their function which limits the portability of the sensor. However, the power requirement is reduced significantly for the recent sensors developed using the nanomaterials.[49] The point-of care and wearable sensors require a self-reliant lightweight power source, which shifts the focus from conventional sensors to TEG-based sensors. The TEG can behave as a transducer and also as an energy source which makes them attractive for the active sensing. The TEG offers poor selectivity for chemical and biosensing. The modification of the active layer with aptamers, antibodies, and enzymes can improve the selectivity of the biosensors. Moreover, the use of hybrid materials and crystalline polymers like metal–organic frameworks (MOFs) as the active layer in the TEG offers different functional groups, pore size, and topology, which can also influence the selectivity of the sensor.

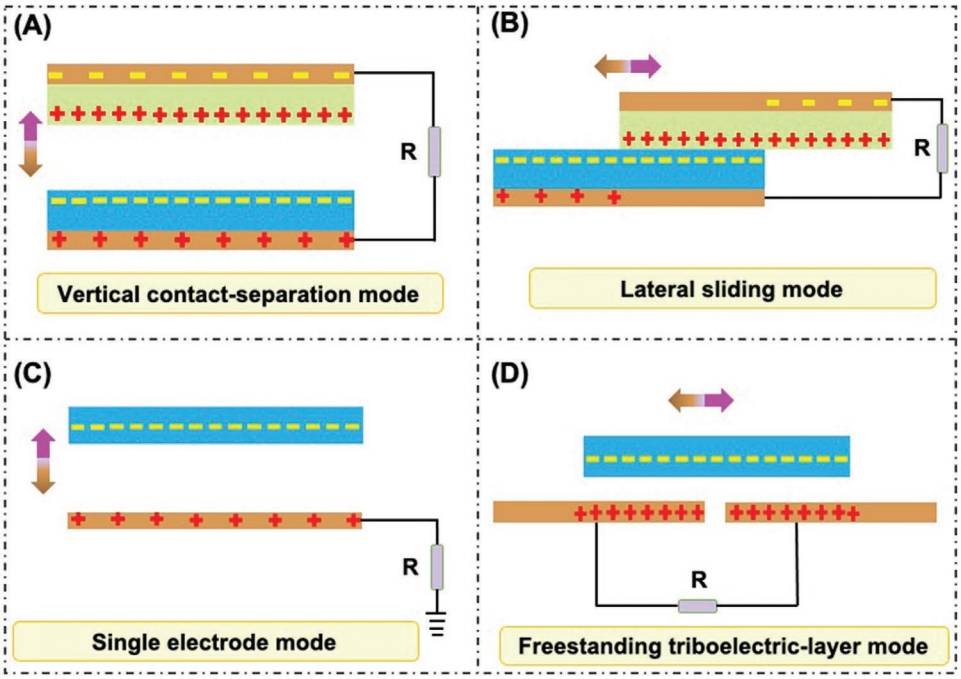

Figure 3. Working modes of TEG. A) Vertical contact-separation mode, B) lateral sliding mode, C) single-electrode mode, and D) freestanding triboelectric layer mode.

4. Physical, Magnetic, and Optical Sensors

TEGs have the ability to convert different mechanical stimuli into electrical signal, which can be used for the real time monitoring of the several parameters of interest. For example, TEG is well reported for the sensing of physical stimulations like acceleration, temperature, strain, pressure, vibration etc. TEG-based physical sensors are covered and discussed in detail in several previous review papers.[17,50] However, for the sake of completion, here we have included a brief summary (**Tables 1–4**) of different TEG-based physical sensors. The key comparison parameters for sensors are working range, sensitivity, resolution (motion sensor) and response/recovery time (tactile, chemical, and biosensors). Sensor that works in wide range can be applied to broader applications. Similarly, sensitivity, i.e., high-output change with the input allows the precise detection of the input compared to the blank. The fast response/recovery time is always desirable for the real-time applications. Thus, these parameters are selected for the comparison in Table 1–4. TEG-based mechanical sensors are generally classified under four categories: i) tactile sensors, ii) pressure sensors, iii) vibration sensors and iv) mechanical motion sensors. Mechanical motion sensors can be used for the rotary, linear, and multidimensional motion sensing.[17] Generally, most TEG-based tactile sensors are associated with pressure sensors. However, tactile sensors essentially need not be a pressure sensor. Tactile sensors can detect different contact parameters including mechanical stimulation (pressure/force), pain and temperature.[51] Mechanical or physical sensors play a vital role in the processing and production lines, intelligent transport systems, equipment fault detection and monitoring, robotics, prosthetics and e-skin applications.[17,52]

Furthermore, physical sensors are also explored as wireless sensor networks (WSNs). The wireless sensor network (WSN) comprising multiple sensor units gained huge attraction due to their use in the smart home, athlete monitoring and environmental monitoring. The major limitation of the WSN is the requirement of sustainable power source. The use of batteries for WSN is challenging as many times it is difficult to track the location of the sensor in a network to replace the batteries. This is where TEG can offer a solution by acting as a sustainable power source to power the sensor or work in conjunction with the batteries to charge them.[53] Moreover, a TEG can also be integrated with signal detection, transmission, or processing modules to develop a self-powered WSN. In this regard, a TEG combined with a power management unit (PMU) and wireless sensor node has been demonstrated for the environmental monitoring by using a commercial sensor.[54] The TEG was also combined with the other electrical components like a switch and an RLC circuit to develop a wireless sensor system that can monitor the speed and the tire pressure of a bicycle.[55] Similarly, the TEG was combined with a PMU, Bluetooth and signal processing unit (SPU), and a heart-rate sensor for designing a wireless body sensor network.[56] The TEG showed feasibility for underwater wireless multisite monitoring of human motions.[57] The key challenge in WSN is to miniaturize and modularize the multiple components involved (transmitter and receiver, SPU, PMU).[53] The TEG performance improvement, manufacturing methods, structure or design optimization are few challenges that need to be focused in the near future. The TEG-based WSN for chemical and biosensing are not explored and it would be interesting to wirelessly transfer the sensing data to a mobile app for the development of self-powered smart sensors. The TEG-based active magnetic and optical sensors are discussed in detail as they are not covered in other review articles.

Table 1. Performance comparison of TEG-based linear, rotary, multidimensional motion sensors.

Type	Device design	Resolution [μm for linear and MDM] [° for rotary]	Measuring Range	Sensitivity	Ref.
Linear motion sensors	LS	0.173	0.005–10 mm s^{-1}	689 ± 4 pA (mm s^{-1})	[18]
	LS	–	V (–0.1 to 0.1 m s^{-1})	–	[58]
	FT (sliding)	250	0.05–0.25 m s^{-1}	–	[59]
	LS	50	50–300 μm s^{-1}	630 μV $μm^{-1}$	[60]
	FT (sliding)	–	3.2–26 mm s^{-1}	–	[61]
	FT (sliding)	2000	25–125 mm s^{-1}	–	[62]
Rotary motion sensors	SE (rotating)	22.5	150–1000 rpm	–	[63]
	FT (rotating)	22.5	200–2200 rpm	–	[64]
	FT (rotating)	9	100–1000 rpm	–	[65]
	LS	3.8	20–60° s^{-1}	–	[66]
	FT (rotating)	0.25	–	–	[67]
	FT (rotating)	2.03 nrad	20–150° s^{-1}	–	[68]
	FT (rotating)	6	10–1000 rpm	–	[69]
	FT (rotating)	–	268–1658 rpm	-	[19]
Multidimensional motion sensors	SE (sliding)	200	–	–	[70]
	SE (sliding)	250	–	–	[71]
	SE (sliding)	–	0.1–0.6 m s^{-1} (linear) 300–700 rpm (rotation)	–	[72]
	SE (sliding)	–	2–100 Hz	15.56 V g^{-1}	[73]
	SE (sliding)	–	<0.05 m s^{-1}	0.45 V mm^{-1}	[74]
	FT (sliding)	–	3.0–40.0 m s^{-2}	0.289 V s^2 m^{-1}	[75]

4.1. TEG-Based Magnetic Sensors

Magnetic sensors have wide range of applications including environment inspection, safety, magnetic compassing, sensing labels, medical tests, current sensing, navigation, antitheft systems and exploration of the minerals.[105] The methods for magnetic field measurement include the Hall effect, superconducting quantum interference devices (SQUIDs), and

Table 2. Performance comparison of TEG-based vibration sensors.

Type	Device design	Resonant f for vibration sensor	Sensitivity	Measuring range	Ref.
Vibration sensors	CS	30	–	0–30 Hz	[76]
	CS	12	–	2–200 Hz	[77]
	CS	15	–	5–80 Hz	[78]
	CS	–	3.65 μW g^{-1}	–	[79]
	FT	–	0.391 V (m s^{-2})	–	[80]
	CS	–	0.26 V s m^{-2}	0–60 m s^{-2}	[20]
	CS	–	6 N mm^{-1}	–	[81]
	CS	–	315 V m^{-1}	0.01–0.11 m	[82]
	CS	16 (Vertical) 8.5 (Horizontal)	–	0–23 m s^{-2} (Vertical) 0–15 m s^{-2} (Horizontal)	[83]
	FT (sliding)	–	6.08 V g^{-1} (X) 5.87 V g^{-1} (Y) 3.62 V g^{-1} (Z) 3.5 mV s^{o-1}	4.87 g (X) 5.06 g (Y)	[84]
	CS	700	0.97 V N^{-1}	50–3000 Hz	[85]
	FT (sliding)	–	223 V m^{-1}	5–200 mm s^{-1}	[86]
	CS	–	20.4 V m^{-1} s^{-2}	1–11 m s^{-2}	[87]

Table 3. Performance comparison of TEG-based pressure sensors.

Device design	Resolution	Sensitivity	Measuring range	Ref.
CS	0.16 Pa	6.9 V kPa^{-1}	–	[22]
SE	–	–	0.0625–0.2815 kPa	[88]
CS	–	8.98×10^{-3} V kPa^{-1}	9.31–46.55 kPa	[89]
CS	8 × 8 pixels	–	–	[90]
SE	15°	3.6 V N^{-1}	0–18 N	[91]

magnetoresistive, flux-gate, magneto-diode, and other effects.[106] These techniques require an external power source, and are complex. A TEG reduces the power-source requirements, which eventually helps reduce the complexity and improve the mobility. Among wide range of materials explored for fabrication of TEGs, multiferroic and magnetorheological materials can be used for the magnetic detection. In this regard, the TEG-based detection of time-dependent magnetic field is noteworthy.[107] The reported TEG-based magnetic sensor works on different principles including the influence of magnetic field on a metal disk over the TEG device, use of magnetorheological elastomers (where magnetic field influences the motion of filler particles) and the Villari effect. **Figure 4**A shows an example of once such self-powered magnetic sensor where a solenoid produces the magnetic field to attract the iron disk placed on the TEG device. The mechanical deformation by the electromagnetic force produces the electric signal from the device. The ln$V$ versus magnetic field (B) curve shown in Figure 4A confirms the linear relationship with a sensitivity of 0.0363 ± 0.0004 ln(mV)/G. The fabricated sensor can also detect the changing rate of the field with a sensitivity of 0.0497 ± 0.0006 ln(mV)/(G/s). The sensor exhibited a resolution of 3 G, response/reset time of 0.13/0.34 s.

TEG-based self-powered magnetic field (MF) soft sensors have also been reported using materials such as magnetorheological elastomer (MRE). One such example is shown in Figure 4B. The MREs are the elastic materials with micro-sized magnetic particles as the fillers.[109] The sensor can detect time varying uniform magnetic field (UMF)[28] due to the movement of magnetized filler particles which form a chain-like structure parallel to the UMF direction. Figure 4B shows that the output voltage of the sensor increases with the MF and the varying voltage signal at different magnetic flux density (with the angle between the film and the field) could be used for direction measurement. The sensor showed a sensitivity of 16 mV mT^{-1} and a response/reset time of 20/30 ms. Another noteworthy addition to the TEG-based magnetic field detection sensors is based on piezo–tribo hybrid nanogenerator.[108] The hybrid nanogenerator, with poly(dimethylsiloxane) (PDMS)–multiferroic material ((1–x)$BaTiO_3$-$x$$ErFeO_3$) composite as the negative triboelectric layer, shown in Figure 4C, produced an output voltage of 320 V and current of 12 µA. The multiferroic material demonstrates the Villari effect, where the permeability of material is altered by the applied stress and hence the electrical performance can be related to the magnetic flux. Figure 4C further depicts the change in the voltage and current with different fields. The hybrid nanogenerator was used to detect the stray magnetic field generated by the electric kettle, hair dryer and electric iron.

4.2. TEG-Based Photodetectors

Photodetectors are devices that converts the light from different spectral region into the electric signal. The ultraviolet (UV) photodetectors have wide range of applications which includes dosimetry (UV exposure of skin), security, communication, environmental monitoring, optoelectronic circuits, and chemical sensing.[110] The conventional self-powered photodetectors are based on either the photoelectrochemical cell or the p–n junction.[111] The photochemical-based photodetectors are

Table 4. Performance comparison of TEG-based tactile sensors.

Device Size (mm × mm)	Device design	Measuring range	Response time (ms)	Sensitivity	Ref.
3 × 3	SE	–	100	0.29 V kPa^{-1}	[92]
–	SE	>2.1 Pa, <40 kPa	<5	0.31 kPa^{-1}	[21]
50 × 5	CS	–	–	0.5–44 mV kPa^{-1}	[93]
4 × 4	CS	–	40	2.82 mV kPa^{-1}	[94]
2.5 × 2.5	CS	1–80 kPa	70	0.06 kPa^{-1}	[95]
–	SE	40–140 N	–	2 mm (position), 0.28 mV N^{-1} (pressure)	[96]
–	SE	1.3–70 kPa	–	0.013 kPa^{-1}	[97]
0.5 × 0.5	SE	–	–	50 dpi	[98]
–	SE	1500 kPa (normal) 0.5–40 N			[99]
20 × 15	CS	0.1–1 N	514 @ 1 Hz	1.76 V N^{-1}	[100]
20 × 20	SE	0–2 kPa, 2–5 kPa	1.4	78.4 kPa^{-1}	[101]
30 × 30	CS	10–800 Pa	–	0.18 V Pa^{-1} (10–80 Pa) 0.06 V Pa^{-1} (80–800 Pa)	[102]
75 × 75 (array)	SE	10–65 kPa	–	0.11 V kPa^{-1}	[103]
5 × 5	SE	5–50 kPa	–	0.063 V kPa^{-1}	[104]

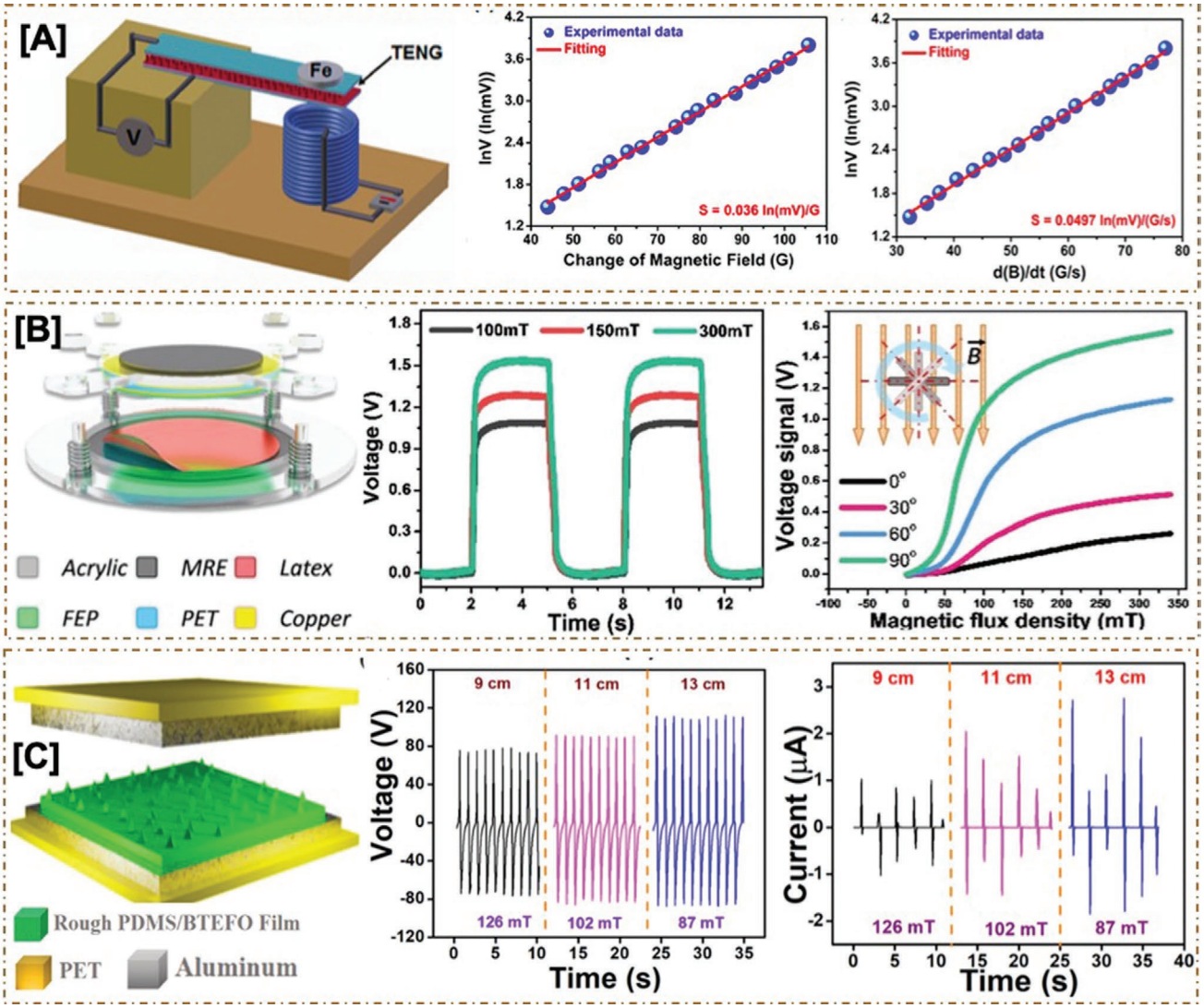

Figure 4. A) TEG as self-powered magnetic sensor with the measurement setup. The plot between the ln*V* versus *B* and ln*V* with the changing rate of the *B*. Reproduced with permission.[107] Copyright 2012, American Chemical Society. B) The design of MRE-based TEG. The variation in the voltage signal of TEG with the different strength transient UMF and the uniformly increased UMF with rotating angle between 90° to 0°. Reproduced with permission.[28] Copyright 2018, Royal Society of Chemistry. C) Design of the hybrid MF-HG device along with the change in voltage and current with varying location of the magnets. Reproduced with permission.[108] Copyright 2021, Elsevier.

not suitable for longer operation and p–n-junction-based photodetectors typically have poor sensitivity at lower light intensity. In comparison, the TEG-based photodetectors are better as in addition to being cost-effective, they show better portability, responsivity, rapid response and decay time, sensitivity and detection range. While the TEG as a power source for photodetector have been extensively explored by the several research groups,[112] only few TEG-based self-powered photodetectors have been reported. The TEG-based photodetector uses a light sensitive material that exhibits the variation in the resistance or the surface potential under illumination, thus altering the output of TEGs. One example of TEG-based portable self-powered active UV photodetector is shown in **Figure 5**A. The devices use TiO_2 dendritic nanostructures as a TEG contact layer.[113] Figure 5A depicts the increasing output current and the decreasing output voltage with increase in the light power density. The photodetector works linearly in the range of 20 μW cm^{-2} to 7 mW cm^{-2} with responsivity of 280 AW^{-1} and exhibited rise/decay time of 18/31 ms. The TEG-based self-powered photodetector using materials such as organometal trihalide perovskite $MAPbI_3$ have been reported too.[29] $MAPbI_3$ is a low-cost, easily processable material which exhibits high light absorption and sensitivity.[114] Figure 5B illustrates the 3D structure of the self-powered photodetector. The variation in the voltage ($V_d - V_l$) increases as the intensity of illumination increases from 20 mW cm^{-2} to 100 mW cm^{-2} (Figure 5B). The device exhibited a responsivity of 7.5 VW^{-1} with a rapid response time of <80 ms. A plasmonic TEG-based photodetector with sensitivity of ≈ 50% has also been reported using GO/Ag heterostructures. The optically active materials like organolead halide perovskites are also used for the fabrication of photo-enhanced TEG.[115] The halide perovskite materials will be the preferred choice for the future TEG-based self-powered photodetector due to their superior properties.

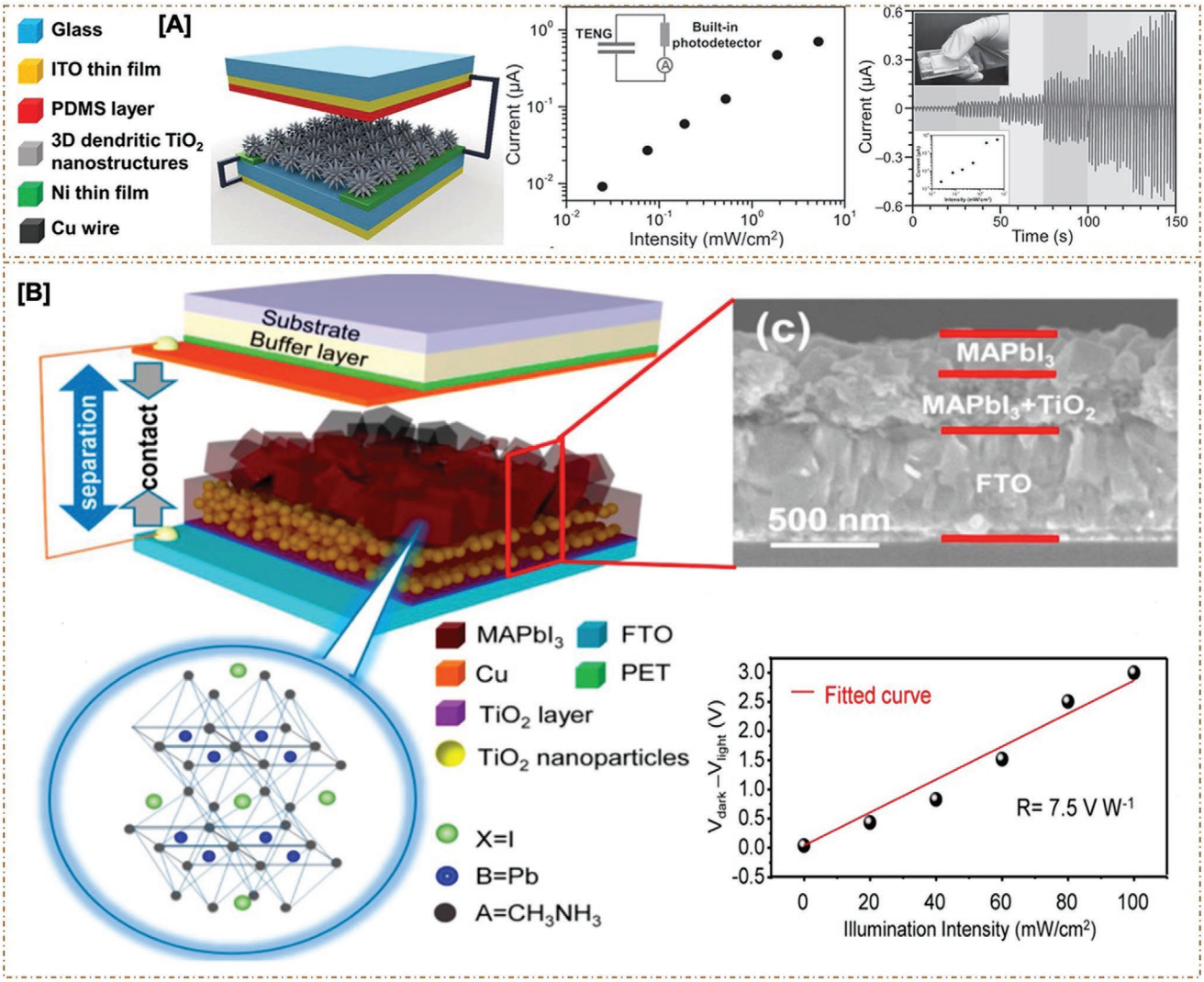

Figure 5. A) 3D illustration of self-powered photodetector with 3D dendritic TiO_2 nanostructures. The change in the current with different intensity of UV illumination and demonstration as stand-alone TEG-based UV photodetector. Reproduced with permission.[113] Copyright 2014, Wiley-VCH. B) 3D illustration of the SPPD with SEM image showing different materials on the FTO. The dependence of the voltage on the illumination intensity. Reproduced with permission.[29] Copyright 2015, American Chemical Society.

5. TEG-Based Self-Powered Chemical Sensors

The TEGs are attractive for active chemical sensing as the active-layer material used for these devices are more likely to interact or absorb with the target molecules.[116] In certain cases, the triboelectric layers are also modified or doped to selectively interact or absorb the target molecule.[17] In simple terms, the target molecule can affect differently the triboelectrification process when compared to the pristine active layer.[44b] The detailed sensing mechanisms of the individual sensors are described in following sub-sections.

5.1. Gas Sensors

The C-S mode TEG with different dielectric materials has been used extensively for the detection of gases such as acetylene, aniline, ammonia etc. The absorption or interaction of the gas molecules with the active layer or preabsorbed species will influence the device output. The majority of chemoresistive gas sensors require complex materials (e.g., $La_2O_2CO_3$, SnO_2) for high selectivity and sensitivity.[117] The synthesis of material generally involves toxic chemicals and solvents (e.g., xylene) which are not eco-friendly.[117a] The gas discharge-based sensors here offer the advantage of no complex material requirement. Like other sensors, gas discharge-based sensors require a power supply, where TEG can also play a major role in sustainable development. Although the TEG as a power source for the sensors is not a focus of this article.

5.1.1. Acetylene Sensors

Acetylene (C_2H_2) is a highly flammable gas widely used for metal welding and cutting. It is also used in the paints, rubber, and fabric industry. Acetylene is toxic due to the traces of arsine

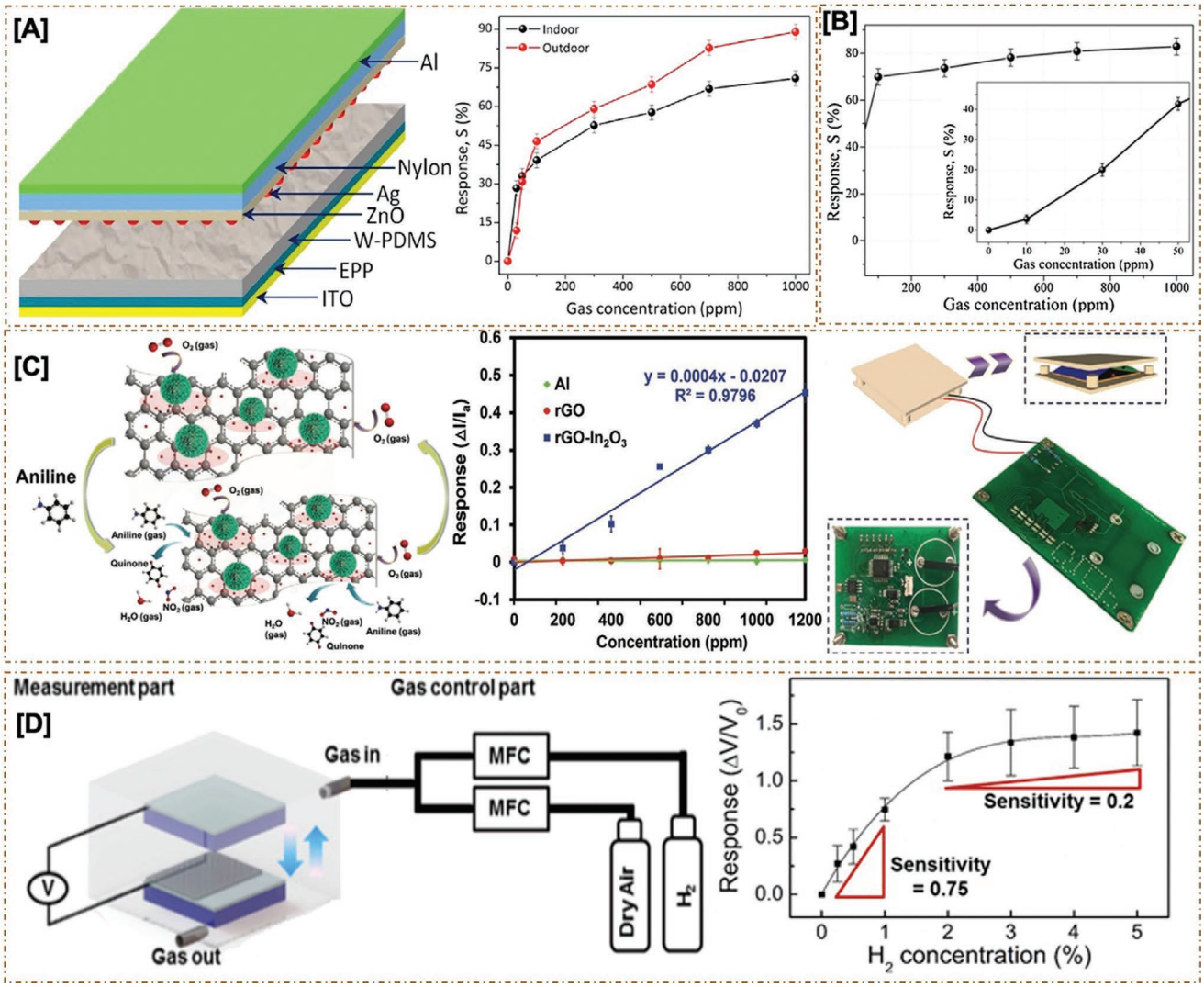

Figure 6. A) TEG device design for acetylene sensing with response of the device for different acetylene concentrations. Reproduced with permission.[119] Copyright 2016, American Chemical Society. B) TEG response for different acetylene concentrations. Reproduced with permission.[120] Copyright 2017, Elsevier. C) Aniline sensing mechanism, device response for different aniline concentrations and self-powered early warning system. Reproduced with permission.[121] Copyright 2020, Wiley-VCH. D) Gas-sensing measurement system and the response of the device toward different H_2 concentrations. Reproduced under the terms of the CC-BY Creative Commons Attribution 4.0 International License (http://creativecommons.org/licenses/by/4.0/).[122] Copyright 2016, The Authors, published by MDPI.

and phosphine generated from calcium carbide.[118] Acetylene can explode at an absolute pressure of >10^3 kPa. Thus, acetylene sensors are important for environmental safety and leakage warning. TEG-based acetylene gas sensors have been reported with wrinkled PDMS (w-PDMS) and nylon as the contact materials.[119] The sensor has ethylene glycol (EG) functionalized PEDOT:PSS (EPP) between the electrode. The w-PDMS layer is used to improve the triboelectric charge transport. In the presence of EPP, the TEG voltage increases from 97.2 to 166.4 V. The EPP films showed improved output under high illumination, as confirmed by the I-V profile. Thus, in the presence of sunlight, the device output further increased to 191.6 V. Similar trend was observed for the current output of the device. The acetylene triboelectric nanosensor (TENS) was fabricated by modifying the upper layer of the TEG device. The top nylon/Al/PET was replaced by the Ag@ZnO/nylon/Al/PET (**Figure 6**A). The Ag contributes to the catalytic activity, and Ag-ZnO heterostructures shows average chemisorption ability. The nylon fibre in the device helps to obtain crumpled Ag@ZnO sensing layer. Figure 6A depicts the response profile at different gas concentrations. The voltage decreases with an increase in C_2H_2 concentration due to the reduced surface charge. The TENS exhibited a maximum response of 89% (outdoor) and 70.9% (indoor) at 100 ppm C_2H_2 concentration. The humidity is well known to influence the output of the TEG. However, in above device, the humidity had a negligible effect due to the shielding by Ag and the high hydrophobicity of w-PDMS.[119] TEGs based on porous PDMS and Al/Ag-CNF have also been reported for acetylene sensing.[120] The response of the one such device is shown in Figure 6B. The output of the device changes in the presence of C_2H_2 due to the surface reaction of the C_2H_2

and the bottom frictional layer. The device exhibited a maximum response of 83% at 1000 ppm C_2H_2 and a response time of 88 s. In this case also, due to the high hydrophobicity of the frictional layers, the humidity did not have any appreciable influence on the performance.[120]

5.1.2. Aniline Sensors

Aniline is a carcinogenic gas that is widely used in laboratories, dying, resins and pharmaceuticals. The aniline vapors are readily absorbed by the digestive tract, skin, and respiratory tract. In worst cases, it can cause carcinogenesis, liver damage and methaemoglobin hematic diseases.[123] Thus, wearable and stand-alone aniline sensors are of great significance and among few TEG examples is the one with low-resistance metal–oxide–semiconductor (MOS) rGO–In_2O_3 electrodes.[121] The sensing operation is due to the change in the conductivity of the electrode and the properties of the frictional layer. rGO is a p-type material where the major charge carriers are defects and vacancies (Figure 6C). Contrary to this, In_2O_3 is an n-type material with free electrons as the dominant charge carriers. In the air, chemisorbed oxygen species (O^-) are formed on the rGO–In_2O_3 surface and in the presence of aniline, the charge-carrier concentration increases as it reacts with the absorbed O^- species.[124] As a result, the resistance of the rGO–In_2O_3 layer decreases and aniline is detected. The process is reversible, and aniline desorbs in the presence of air. Figure 6C depicts the response of the Al-TEG, the rGO-TEG, and the rGO–In_2O_3 TEG at various aniline concentrations. The rGO–In_2O_3 TEG works well in the linear range of 200–1200 ppm. The device has a response time of 350 s and has a shorter recovery time. The interference studies confirm the sensor's selectivity as the response was poor in the presence of other volatile gases. The sensor works well in the humidity range of 35–48%. Figure 6C also shows the integration of the rGO–In_2O_3 TEG with circuits and LEDs to demonstrate the early warning system.[121]

5.1.3. Hydrogen Sensors

Hydrogen (H_2) can replace fossil fuels, but it is highly flammable and explosive. The effective and efficient detection of H_2 is important to ensure human and environmental safety.[125] One example of TEG here is based on palladium (Pd) and PET active layers. Pd is widely reported for highly selective and sensitive H_2 sensing.[122] The H_2 absorbed on the Pd molecules expands the volume of the Pd and transforms to β-phase or α-phase palladium hydride (PdH_x) depending on the H_2 concentration. Therefore, in the presence of H_2, the electrical and optical properties of Pd get altered. Figure 6D shows the measurement setup, comprising a chamber and mass flow controller (MFC) connected to dry air and H_2 gas. The PdH_x formed in the presence of H_2 has a lower work function compared to that of Pd. The output voltage of TEG thus increases in the presence of H_2 as the work function of PdH_x is closer to the PET donor states resulting in the improved charge exchange. Figure 6D depicts the sensor response at different H_2 concentrations. The sensor exhibited a sensitivity of 0.75 up to 1% H_2 and 0.2 above 2% H_2 exposure. The sensor has a response time of 30 min and a recovery time of 15 min under 1% hydrogen exposure.[122] Due to longer response and recovery time, this sensor is unsuitable for practical applications.

Another example of a TEG-based hydrogen sensor uses micropyramid PDMS and Pd-decorated ZnO nanorods as the negative and positive triboelectric layers, respectively.[126] The device produced an output of 5.2 V and 80 nA. **Figure 7**A illustrates the H_2 sensing mechanism. The oxygen ions ($O_{2(abs)}$) are chemisorbed on the Pd in the presence of air. The electrons migrate from ZnO to Pd due to the higher work function of Pd. In the presence of H_2, the H_2 molecules react with the absorbed O^-, leading to the formation of H_2O and release the electrons back to ZnO. The movement of electrons modify the Pd/ZnO interface and lower the barrier width, thus reducing the TEG voltage by screening the triboelectric field.[127] Figure 7A shows the output voltage and response of the device at different H_2 concentrations. The device exhibited a response of 373% at 10 000 ppm H_2 and a response time of 100 s at 5000 ppm. The device response is faster at lower concentrations. The effect of humidity was also studied. Later micropyramid PDMS was replaced with the w-PDMS for the H_2 sensing (Figure 7B).[128] The device generated an output of 16.2 V and 0.512 µA. The device showed the detection limit, recovery-response time, and the response of 20 ppm, 115–126 s, and 1457.69%, respectively. A corrugated core sandwich (CCS) TEG (CCS-TEG) is yet another example for H_2 sensing.[116a] Figure 7C shows the CCS-TEG structure, with Pd coated on the polyimide (PI) for the sensing. The effect of the crosswise and length-wise assemblies on the TEG output was also analyzed. The crosswise assembly TEG produced an output of 142 V and 9.3 µA. The stacked CCS-TEG (4 devices) was used for the H_2 sensing. Figure 7C also depicts the generated output and response of the sensor at various H_2 concentrations. The sensor has a detection range of 0.001–1.00 vol.% with maximum response of 83%.[116a]

5.1.4. Ammonia Sensors

Ammonia (NH_3) is one of the toxic air and water pollution contributor and can cause acute damage to humans.[130] It can induce headaches, nausea, pulmonary damage and even cause death at higher concentrations.[130c] Ammonia can contaminate water, and it can also exist in the atmosphere as the suspended particles. On other hand, NH_3 present in the exhaled gas can also act as a marker to detect kidney diseases.[131] In terms of active sensors for detection of ammonia, TEGs based on polyaniline (PANI) nanofibers (NFs) and poly(vinylidene difluoride) (PVDF) active layers have been reported.[129] The PANI NFS plays the role of the electrode, frictional layer, and sensing layer. PANI can exist as conducting emeraldine salt (C-PANI) and non-conductive emeraldine base (N-PANI), reversibly convertible by deprotonation and protonation. The analysis of the effect of the PANI's state on the TEG performance shows that C-PANI TEG can produce better output (1186 V and 45.70 µA) due to high surface charge density and hence preferred for NH_3 sensing. The conductivity of C-PANI changes in the presence of NH_3 and thus can alter the output of the C-PANI TEG. The C-PANI can transform to the N-PANI by the absorption of NH_3

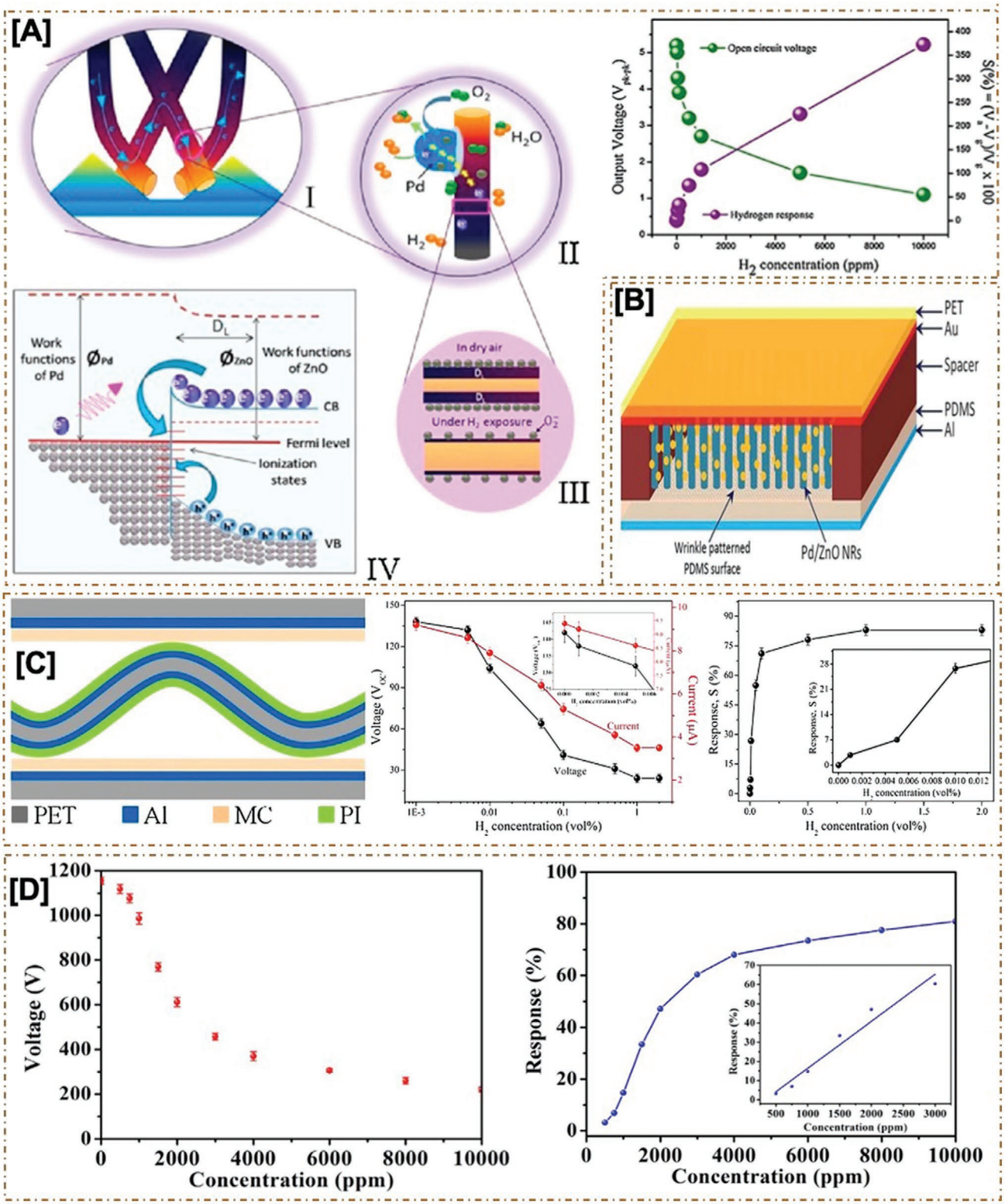

Figure 7. A) Schematic illustration of the H_2-sensing mechanism and response of the sensor. Reproduced with permission.[126] Copyright 2016, Elsevier. B) 3D illustration of the TEG device with w-PDMS and Pd/ZnO nanoparticles as the active layer. Reproduced with permission.[128] Copyright 2016, Royal Society of Chemistry. C) The CCS-TEG device design. Variation in the voltage/current and response of the device at different hydrogen concentrations. Reproduced with permission.[116a] Copyright 2017, Elsevier. D) Voltage and response of the TEG-based ammonia sensor in the concentration range of 500–10000 ppm. Reproduced with permission.[129] Copyright 2018, Elsevier.

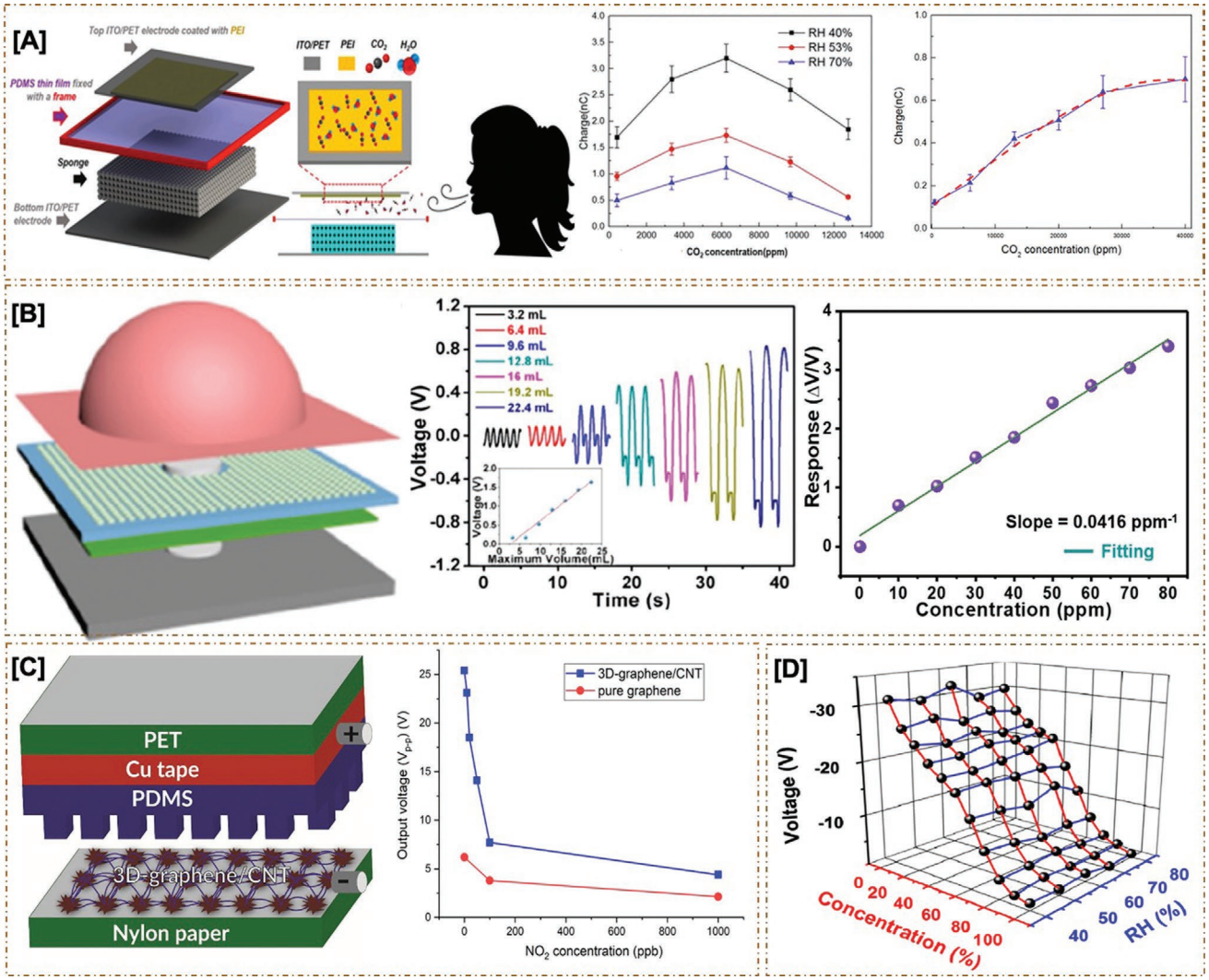

Figure 8. A) Exploded view of the WATEG and the concept of CO_2 sensing. The charge versus CO_2 concentration profile of the sensor at different RH and the linear working range of the sensor. Reproduced with permission.[133] Copyright 2017, American Chemical Society. B) Schematic representation of AIMS. The variation in the voltage with different air volume and NO_2 concentrations. Reproduced with permission.[23] Copyright 2020, American Chemical Society. C) Design of the self-powered NO_2 sensor based on the 3D-graphene/CNT. The variation in the output voltage with NO_2 concentration in the range of 0–1000 ppb. Reproduced with permission.[136] Copyright 2021, Elsevier. D) The output voltage versus concentration and relative humidity curve for ethanol solution sensing. Reproduced with permission.[27] Copyright 2013, Elsevier.

on its surface. Figure 7D shows the variation in the voltage and response of the device with NH_3 concentration ranging from 500 pm to 10 000 ppm. The device exhibited a linear response up to a concentration of 3000 ppm. The saturation of absorption sites at higher concentrations results in a non-linear response (Figure 7D). The device has a response time of 40 s and a recovery time of 225 s. This highly selective sensor shows poor response from other interfering molecules like ethanol.[129]

5.1.5. Carbon Dioxide Sensors

Carbon dioxide (CO_2) is a greenhouse gas that plays a role in climate change and is used in wider range of applications such as pest control, carbonated drinks, plant growth, oil recovery and medical sector etc.[132] CO_2 sensors are important to monitor air quality to maintain environmental standards and safety. A few examples of TEG-based CO_2 sensor include the water–air TEG (WATEG), as shown in **Figure 8**A.[133] The polyethyleneimine (PEI) layer in this TEG acts as a selective sensing material for CO_2 detection. The device is designed to create a force and humidity independent charge transfer process, which is critical for the practical implementation of the sensors. The upper PEI and PDMS layers in the device work in constant contact while the wetted sponge and PDMS contact are force-dependent. Figure 8A explains the CO_2-sensing mechanism where a carbamate layer is formed due to the CO_2–PEI complexation. The CO_2 absorption alters the electronegativity of the sensing layer to influence the output of the device. For static CO_2 sensing, the PEI layer is exposed to CO_2 at controlled RH in a sealed chamber for 30 min. The sensing material was removed from the chamber and used in the WATEG for the measurements.

As the only PEI layer playing a role in sensing, the top contact output only changes with the CO_2. Figure 8A shows the change in charge profile with CO_2 concentrations during static sensing. The charge versus concentration curve suggests that carbamate is not the only factor influencing electronegativity, and other participating species are absorbed. The sensor exhibits a sensitivity of 4.8×10^{-4} nC ppm^{-1} (40% RH) in the CO_2 concentration range of 400–2000 ppm. For dynamic testing, gas spray (1000 mL) with different CO_2 concentrations was used. Figure 8A depicts the charge versus concentration profile for the dynamic sensor. The sensor range is increased to 30 000 ppm, after which the output saturates. The dynamic sensor is also useful for the measurements in the environment with different RH values.

5.1.6. Nitrogen Dioxide Sensors

Nitrogen dioxide (NO_2) generated from the vehicle and other fossil fuels combustion is responsible for water pollution, ozone formation, and acid rain.[134] A persistent NO_2 exposure of ≈100 µg m^{-3} could lead to severe respiratory diseases.[135] The NO_2 exposure causes chronic obstructive pulmonary disease (COPD) in nearly 63% adult population of the United States.[23] The TEG offers a promising solution for the development of stand-alone battery-free NO_2 sensors.

An example of a TEG-based NO_2 sensor, shown in Figure 8B, uses alveolus-inspired membrane (AIM) for NO_2 sensing and human-breath analysis.[23] The tungsten trioxide treated with NaOH was used in this device as the sensing material. Figure 8B also depicts the output voltage and response of the sensor in the concentration range of 0–80 ppm. The voltage output at different volumes of the injected air changes linearly with the gas flow. The sensor demonstrated a response, response time and recovery time of 340.24%, 273 s, and 330 s, respectively. The device maintains the same response for a month with a minor change of 5% at each level. The theoretical studies, including phase-field simulation, thermodynamic analysis and finite element calculations, revealed the sensing mechanism. The electrical output is increased in the presence of NO_2 due to the capture of electrons, resulting in the reduced depolarization field in the WO_3-sensing layer.[23]

Another TEG sensor, capable of detecting NO_2 gas at sub-ppb level, uses patterned PDMS as the negative and 3D-graphene/CNT or graphene as the positive triboelectric layer.[136] Figure 8C depicts the 3D schematic of the device. The 3D-graphene/CNT produced a higher voltage (25.4 V) than graphene (6.2 V). The output of the device reduces with the increase in the NO_2 concentration (Figure 8C). The voltage variation is ascribed to the change in the resistance of the sensing layer. The 3D-graphene/CNT showed a response in the range of 10–1000 ppb, while graphene showed a response at a concentration higher than 100 ppb. The sensor exhibited good selectivity for the NO_2 compared to the interfering H_2, CO, and CO_2 gases.[136]

5.1.7. Automotive Exhaust Sensors

Growing use of automobiles is also contributing carbon monoxide (CO), VOCs, NH_3 and nitric oxide (NO) to the environment and adversely affecting human health and climate neutrality.[137] TEG-based sensors could offer attractive solutions for detection of emitted gases. The examples of TEG-based gas sensors include the one based on polypyrrole (Ppy) derivatives and PDMS for NO, CO and NH_3 sensing.[138] The pipe-shaped device consists of seven sensing units with different Ppy derivatives, created using different dopants. The sensing units are Ppy-SBS (sodium benzene sulfonate), Ppy-CSA (camphor sulfonic acid), Ppy-SDS (sodium dodecyl benzene sulfonate), Ppy-SO (sodium oxalate), Ppy-OA (oxalic acid) and Ppy-NSA (naphthalene sulfonic acid). The sensing signal depends on the interaction of Ppy with the gases. The charge density decreases in the case of NH_3 as it is a reducing gas. NO being an oxidizing gas increases the concentration of charge carriers. Hence, both have opposite effects, i.e., NH_3 increases the resistance while NO improves the conductivity. The response-recovery time for CO in the Ppy-CSA-based sensing unit is 11–5 s; for NO in the Ppy-SBS-based unit is 31–30 s; and for NH_3 in the Ppy-NSA-based unit is 13–12 s. The influence of humidity was also tested. The response to NH3 increases even at high humidity which suggest the suitability of the sensing unit at high humidity. The device was also tested for real-time automotive exhaust monitoring by placing it in different types of vehicles (sedan and sports utility vehicle (SUV)).[138] The device detects the different concentration of exhaust emission from sedan (more NO) and SUV (more CO and NH_3).

5.1.8. Volatile Organic Compounds Sensors

Volatile organic compounds (VOCs) such as benzene, toluene, ethanol, acetone, methanol, etc., are toxic and directly affect human health.[4a] VOCs, enter the environment from various sources, including building materials, adhesives, and paints.[139] The consumption of a high amount of ethanol is associated with accidents and social abuse.[140] Benzene and toluene are more toxic, carcinogenic and can cause confusion, headache, dizziness, and blurred vision.[141] Thus, detection and monitoring of the VOCs in the environment are essential for better human health. TEG-based sensors with polyamide/Al and poly(tetrafluoroethylene) (PTFE)/Al as the contact layers have been reported for the liquid and gas sensing respectively.[27] Water and ethanol were selected in these cases for liquid and gas sensing. Figure 8D depicts the relationship between the voltage of PTFE–TEG and liquid ethanol concentration. The output voltage decreases with the increase in the ethanol concentration. The figure reveals that RH slightly influences the PTFE–TEG sensor performance.[27]

A vapor-actuated perfluorosulfonic acid ionomer (PFSA) was used to fabricate the bendable TEG (**Figure 9**A) for vapor (acetone, n-hexane, ethanol etc.) leak detection in the vapor pipeline.[142] The vapor responsive behaviour of PFSA was due to the presence of nanochannels inside the membrane. The nanochannels expand with the absorption of moisture or vapor molecules and vice versa. The expansion or shrinkage of the nanochannel deforms the blade to drive TEG. The developed TEG can harness energy from wind and water drops. The device has a power density of 1.6 W m^{-2} at a wind speed of 25 ms^{-1} and 230 mW m^{-2} at a water drop rate of 2 mL s^{-1}. Figure 9A shows the change in PFSA sensor signal with different vapors. The

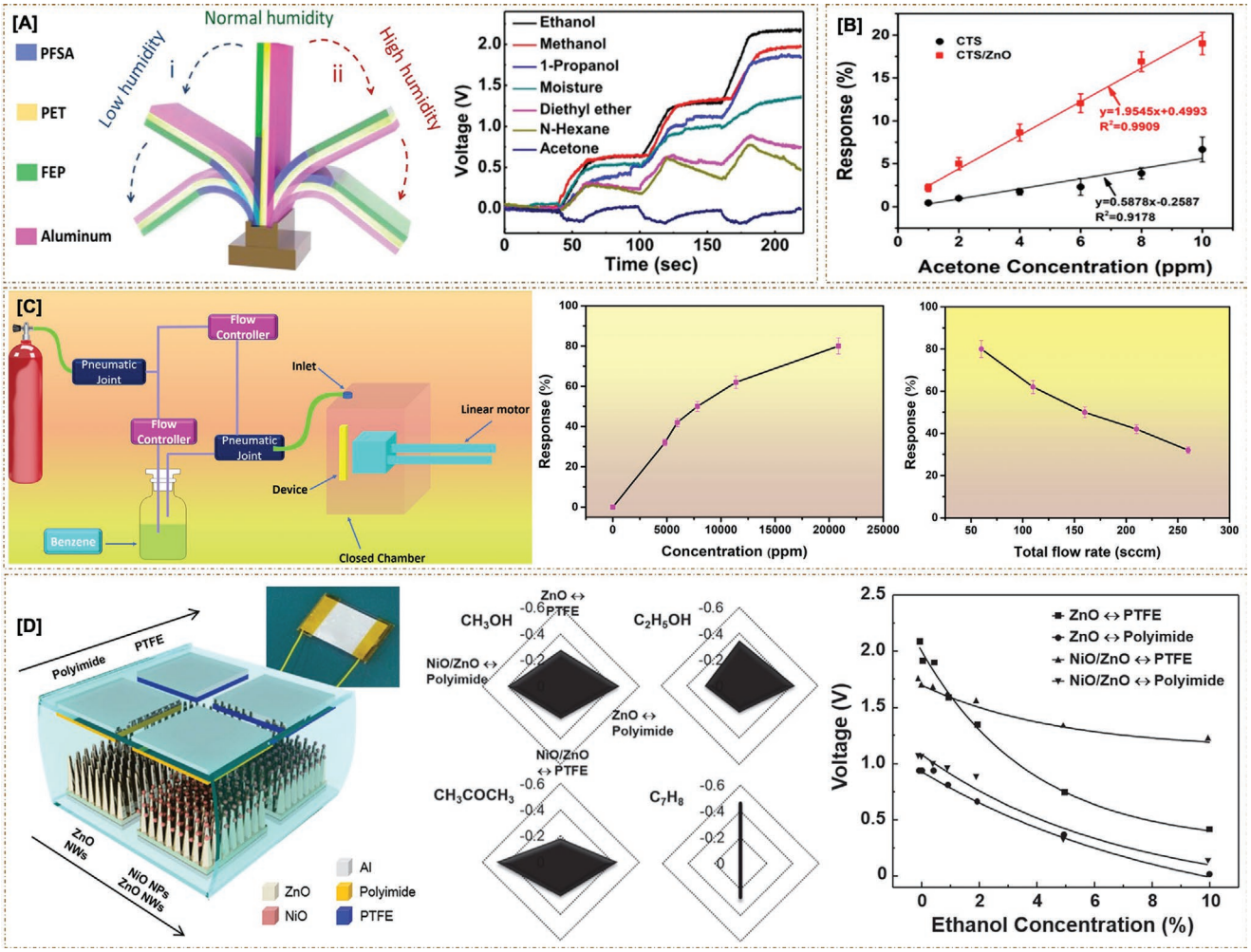

Figure 9. A) The humidity-resistant TEG device design. The output voltage signal in the presence of various VOCs. Reproduced with permission.[142] Copyright 2019, American Chemical Society. B) Device response toward different acetone concentrations. Reproduced with permission.[145] Copyright 2020, Elsevier. C) The lab-designed benzene vapor generation and the device testing system. The response of the device across different benzene concentrations and total flow rate. Reproduced with permission.[146] Copyright 2018, Elsevier. D) 3D representation of the electronic nose, radial plots of different VOCs. The output voltage of different sensor elements toward ethanol concentrations. Reproduced with permission.[147] Copyright 2015, Wiley-VCH.

ethanol shows the best response while there is a minor signal change in the presence of acetone vapor.

The acetone in the exhaled breath can also act as a biomarker for prediabetic conditions. For example, the acetone concentration in the breath of a healthy individual varies between 0.3–0.9 ppm and it can exceed 1.8 ppm in the breath of prediabetic patients.[143] With coupled chemisorption and contact electrification it is possible to have self-powered acetone sensor (WSAS) for breath analysis.[144] The humidity tolerant triboelectric acetone sensor (TAS) was fabricated with CS/ZnO bilayer performing the role of the triboelectric and the sensing layer.[145] The CS/ZnO device shows better performance compared to the CS alone. The microstructure PDMS in this device behaves like the opposite contact layer. The CS/TEG showed little variation with humidity due to the presence of inadequate water absorption sites. Figure 9B depicts the response of CS and CS/ZnO TAS in the concentration range of 1–10 ppm. The CS/ZnO TAS exhibited better sensitivity and response of 1.9545% per ppm and 19.02%, respectively, at 10 ppm acetone. The CS/ZnO TAS has a response time of 1883 s and a recovery time of 3635 s. The recovery time of CS/ZnO TAS was higher than that of CS TAS. The TAS was selective with poor response from other exposed biomarkers. In the presence of acetone, the output increases due to the vaporization of the water molecules. The acetone reduces the resistivity of the junction (ρ_{CS-ZnO}).

A TEG-based self-powered benzene sensor, which works in the high concentration range to supplement the currently available benzene sensors (0–100 ppm) has also been reported.[146] The TEG was fabricated by the PVDF–TiO_2 and cellulose acetate as negative and positive triboelectric layers respectively. The output of TEG was improved by employing the phase inversion process for the PVDF–TiO_2. The phase-inversed PVDF-TiO_2 (10 wt%) based TEG showed 10- and 7-times enhancement in the output current and voltage, respectively. Figure 9C demonstrates the as-fabricated TEG for benzene sensing and warning

system using a custom-designed setup. The output of the device decreases with the increase in the benzene concentration. The voltage change was attributed to the alteration of the local density of states by the interaction of C p-states and the d-states of the Ti. The interaction restricts triboelectrification.[148] Figure 9C shows the device's response concerning the benzene concentration and total flow rate, respectively. The sensor was selective and exhibited a sensitivity of 0.0035 V ppm^{-1} concerning concentration. The device was also integrated with the Arduino-Uno for displaying a warning message and trigger the alarm.

An electronic nose designed to detect different VOCs (toluene, methanol, acetone, and ethanol) is shown in Figure 9D.[147] The TEG-based e-nose uses ZnO nanowires (NW) or ZnO NWs with NiO nanoparticles as one layer and polyimide (PA) or PTFE as the opposite contact layer. The *I*–*t* analysis confirmed that ZnO NWs show significant current changes for acetone but not for other gases. The ZnO NWs decorated with NiO showed better sensitivity due to the formation of the p–n junction. The formation of the p–n junction increases the resistance of the oxides. Figure 9D represents the radial plot of four VOCs for different systems. The variation in the output voltage of TEG with ethanol concentration in the range of 0.1–10% for different systems is shown in Figure 9D. The sensor exhibits a detection limit of 0.1%. The similar properties of methanol and ethanol give rise to similar radial plots. Thus, a greater number of sensor elements are needed to differentiate similar gases. The response of PA-based sensor was faster than a PTFE-based sensor. **Table 5** shows the comparison of the TEG-based active gas sensors discussed in above sections.

5.2. Heavy-Metal-Ion Sensors

Heavy-metal ions like mercury (Hg^{2+}), lead (Pb^{2+}), chromium (Cr^{+3}) etc., are highly toxic and non-biodegradable and pose a great threat to the environment and human health.[149] Water contamination by activities in the mining, paper, metal plating, and battery industries is also leading to rising heavy metal ions in water and, as a result considerable efforts have been made for the detection and removal of heavy metal ions.[150] However, most of the detection and removal techniques are expensive, energy-intensive and time-consuming and TEG-based approach can be a better alternative. As a result, TEGs have been explored by many researchers for the detection and removal of heavy metal ions. Examples include detection of mercury compounds, which can cause Minamata disease by affecting cognitive abilities, memory, and language.[149b,151] The TEG-based approach can overcome the challenges faced with conventional techniques. For example, the spectrometry methods are highly selective for mercury ion detection but suffer from high-cost, complicated sample preparation and are incompetent for field analysis. The other complicated methodologies that provide high sensitivity and selectivity involve surface-plasma resonance (SPR), colorimetric assays, electrochemical sensors, surface-enhanced Raman scattering.[152]

In this direction, the enhanced output TEG, designed as a self-powered Hg^{+2} ion sensor, in noteworthy.[153] The performance of TEG was enhanced by depositing gold (Au) nanoparticles (NP) on the metal plate, which eventually increases the effective contact area. The Au NPs of size 13, 32, and 56 nm were prepared on the Au film. The Au NPs were modified further with 3-mercaptopropionic acid (3-MPA) to provide sensitivity and selectivity for Hg^{+2} ion detection. The TEG follows an output trend of $TEG_{56nm} > TEG_{32nm} > TEG_{13nm} > TEG$. The 56 nm Au NPs modified TEG produced 5- and 6.8-times higher voltage and current density, respectively (**Figure 10**A). The carboxylic acid group of 3-MPA has a high binding ability toward the Hg^{+2}, leading to the change in the nanogenerator output. The Au plate was dipped for 60 min in the solution containing different concentrations of Hg^{+2} ions for the sensing. The electrical measurements were performed after washing and drying at ambient temperature. Figure 10A depicts the variation of the short-circuit current ratio with the mercury ion concentration. Figure 10A suggests the selectivity of the sensor as there is no interference of the other metal ions. The developed sensor exhibited an R^2 of 0.98 in the concentration range of 100×10^{-6} M to 5×10^{-6} M with a detection limit of 30×10^{-9} M (S/N = 3).

Moreover, a fully standalone sensor was demonstrated by using a light-emitting diode (LED). The LED was unable to

Table 5. Comparison of different TEG-based active gas sensors.

Sensor	Negative TE layer	Positive TE layer	Range	Response time (s)	Recovery time (s)	Ref.
Acetylene	Wrinkled PDMS	Nylon	300–1000 ppm	–	–	[119]
Acetylene	Porous PDMS	Al/Ag–CNF	10–1000 ppm	88	120	[120]
Ammonia	PVDF	PANI	500–3000 ppm	40	225	[129]
Aniline	rGO–In_2O_3/PVDF	Al	200–1200 ppm	200	–	[121]
H_2	Wrinkled PDMS	Pd NPs/ZnO nanorods (NRs)	0.01–3 vol.%	115	126	[128]
H_2	PDMS	ZnO NRs	100–10 000 ppm	100	–	[126]
H_2	PI	Microcrystalline cellulose	0.001–1.0 vol.%	82	99	[116a]
Acetone	PTFE	Nylon	0–10 ppm	–	–	[144]
Acetone	PDMS	Chitosan/ZnO	1–10 ppm	–	–	[145]
NO_2	Latex	WO_3	0–80 ppm	273	330	[23]
NO_2	PDMS	3D graphene/CNT	10–1000 ppb	–	–	[136]
Benzene	PVDF–TiO_2	Cellulose acetate	4814–20 861 ppm	–	–	[146]

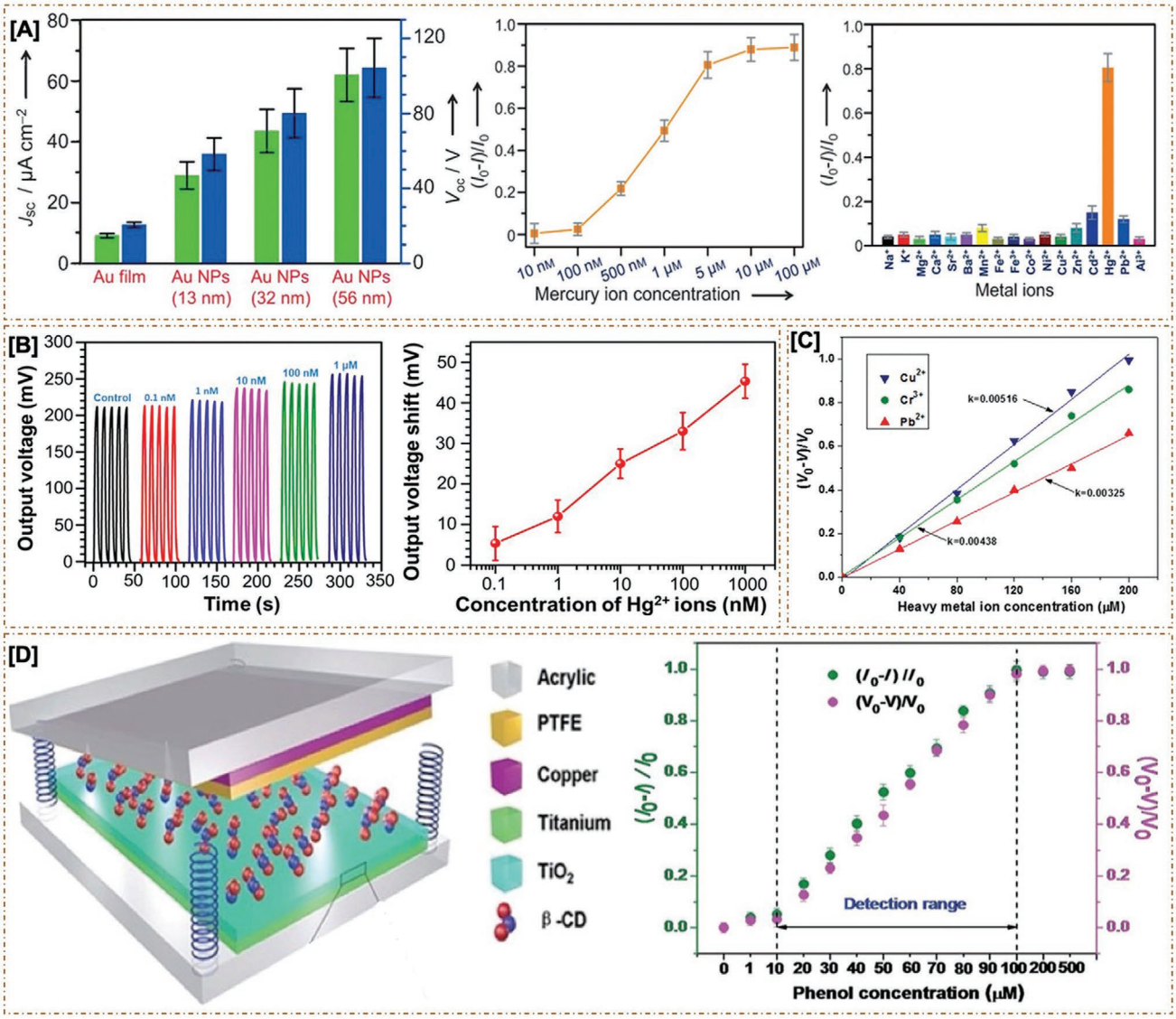

Figure 10. A) The performance (V_{oc}, J_{sc}) for gold film and different size gold nanoparticles. Short-circuit current ratio for different Hg^{+2} ion concentrations and sensor selectivity. Reproduced with permission.[153] Copyright 2013, Wiley-VCH. B) The output voltage and voltage shift for different Hg^{+2} ion concentrations. Reproduced under the terms of the CC-BY Creative Commons Attribution 4.0 Attribution license (https://creativecommons.org/licenses/by/4.0/).[25] Copyright 2020, The Authors, published on behalf of The Electrochemical Society by IOP Publishing Limited. C) Open-circuit voltage ratio at different concentrations of Cu^{+2}, Cr^{+3}, and Pb^{+2} heavy metal ions. Reproduced with permission.[154] Copyright 2016, Wiley-VCH. D) 3D representation of β-CD enhanced TEG for phenol detection. Short-circuit current and voltage ratio for phenol in the concentration range of 0–500 × 10^{-6} M. Reproduced with permission.[26] Copyright 2015, Royal Society of Chemistry.

glow when the layer was treated with 5×10^{-6} M Hg^{+2} ion. Similarly, the Au NPs were capped with MPA to demonstrate single electrode solid–liquid contact electrification-based Hg^{+2} ion triboelectric nanosensor (TNS).[25] Unlike a solid–solid contact sensor, this sensor is independent of the contact frequency for mercury ion detection. The MPA capped Au NPs were synthesized on the copper wire. Figure 10B depicts the output voltage and calibration curve at different concentrations of the Hg^{+2} ions. Like a solid contact sensor, the MPA has a strong binding affinity to mercury ions. The Hg^{+2} binding to MPA reduces the work function as confirmed by the Kelvin probe force microscopy (KPFM). The reduced work function can lead to improved charge transfer during the electrification process. The designed TEG can work in the linear range of 10×10^{-9} M to 1×10^{-6} M with a 10×10^{-9} M detection limit.

The triboelectric effect has also been employed for detection and removal of heavy metal ion such as Cu^{+2}, Pb^{+2}, Cr^{+3}.[154] The multilayered structure TNS developed to detect Pb^{+2}, Cr^{+3}, and Cu^{+2} as common contaminants in industrial wastewater. The TNS consists of a top PTFE layer with (NW) array and bottom layer of surface grown anodized aluminium oxide (AAO) on Al foil. The AAO nanopores were modified with the sodium diethyldithiocarbamate, dithizone, and diphenylcarbazide for selective recognition of Cu^{+2}, Pb^{+2}, and Cr^{+3} respectively. Figure 10C shows the variation in open-circuit voltage ratio with the concentration of Cu^{+2}, Cr^{+3}, and Pb^{+2}. The modifications of

AAO nanopores make the TNS highly selective and specific for each heavy metal ion. The TNS showed a sensing range of 0–200 × 10^{-6} M for all three metal ions. The TNS exhibited a sensitivity of 0.004 × 10^{-6} M, 0.005 × 10^{-6} M and 0.003 × 10^{-6} M for Cr^{+3}, Cu^{+2}, and $Pb^{+2,}$ respectively. The sensor also exhibited excellent reusability.[154] Moreover, wastewater-driven rotating TEG (WD-TEG) was developed and demonstrated to remove heavy metal ions.[154]

5.3. Phenol Liquid Sensors

Phenol is highly toxic and has adverse effects on the respiratory tract, human eyes and the skin. Repeated or continuous exposure to phenol can severely effect the central nervous system (CNS), liver, heart and kidneys.[155] Phenol also has a negative impact on the environment and biological communities. Like other analytes discussed above, it can also be detected by conventional techniques such as chromatography, electrochemical and spectrophotometric methods.[156] However, the TEG-based approach is more attractive due to self-powering, simplicity and portability. An example of PTFE and TiO_2 NWs as the active layers in a TEG for the detection of phenol is shown in Figure 10D. [26] The TEG has TiO_2 NWs modified with the β-cyclodextrin (β-CD) to enhance the device output. Additionally, β-CD plays the role of recognition molecule or element as its cavity size is appropriate for phenol absorption. The device with 80 × 10^{-6} M β-CD showed 8.7 times and 6 times enhancement in the voltage and current, respectively. The voltage and current output of this device decrease in the presence of phenol as it leads to poor electron transfer. Figure 10D shows the variation in the voltage and current ratio at various phenol concentrations. The sensor exhibits a sensitivity of 0.01 × 10^{-6} M in the concentration range of 10 to 100 × 10^{-6} M. The sensor is highly selective toward phenol detection with poor response to other organic species. The sensor is reusable by rinsing with ethyl alcohol. Moreover, the enhanced output TEG with the modified design was also demonstrated for the electrochemical degradation of the phenol in wastewater. The kinetic impact of the water waves brings the device in contact separation. The 90% phenol degradation was observed in 320 min.[26]

5.4. Thioacetamide Sensors

Thioacetamide (TAA) is another toxic contaminant from the rubber, paper, textile, and leather industries.[24] It can cause liver carcinogenic and neurotoxic injuries by inhibiting the activity of the DNA and the RNA.[157] The effluent from industries containing TAA can easily contaminate the water. In humans, TAA can be metabolized rapidly for the generation of reactive metabolites.[158] The TEG-based sensors for TAA has been reported using biocompatible metal biomolecule framework (MBIOF). The TEG comprises Cu-Asp nanofibers developed using a green synthesis route.[24] Additionally, Cu-Asp can be coated on various substrates using an easy to scale-up tape cast coating technique. The coated nanofibers remain stable in water. The TEG produced 200 V in freestanding mode (NF-TEG) and 80 V in C-S mode (cNF-TEG). The 1 cm × 1 cm cNF-TEG can be used to sense TAA and this is been demonstrated (**Figure 11**A) by dropping 20 µL volume of the different TAA concentrations (1 × 10^{-3} to 100 × 10^{-3} M) on the Cu-Asp nanofiber. The decreasing voltage in Figure 11A is due to the decrease surface potential of the copper thioacetamide complex formed after adding TAA. The sensor was selective and exhibited a sensitivity of 0.76 V mM^{-1}. **Table 6** summarizes the TEG-based active liquid sensors like heavy metal ions, phenol and thioacetamide sensor discussed in section 5.2–5.4.

As discussed above, gas detection mainly utilizes contact-separation mode TEGs with different dielectric materials. The excellent diffusion performance of gases allows their uniform distribution over the device active layer to influence the device output. The TEG is explored as an active sensor for numerous gases, with gas chamber used to precisely controlled the environment. However, the use of gas chamber is not feasible when it comes to bringing the utilization of TEG-based sensors in real-time applications. Significant efforts are required to design a fully packed and portable TEG-based gas sensor. Moreover, the response of sensors is affected by the humidity, which opens up the scope for research in humidity resistant materials. The key considerations for commercialization of TEG-based sensors are stability, reusability and high selectivity. Although many reported sensors claimed excellent sensitivity the detection of complex analytes by TEG-based sensors is still a challenge which can be resolved by using highly selective sensing material as active layer. In the case of gas and liquid analytes, most of the reported sensors are not reusable, which means the signal cannot return to the initial state in the absence of the analyte. Reusability requires the removal of absorbed molecules from the sensing layer, which is generally achieved by heating, washing, or purging the air. All these methods restrict the application of the device. Considering this background, novel materials such as MXenes and MOFs have been explored recently for the active layer of TEGs. The feasibility of MOFs has been demonstrated for TEG-based sensors which can be reused after a simple washing process. These materials can also be explored for chemical sensing using a reusable, sensitive and highly selective TEG-based active sensor. Alternatively, photocatalytic degradation of the analyte can be explored for the fabrication of a reusable sensor. Despite few successes related to TEG-based chemical sensors, lot more need to be done to impart reusability and high selectivity.

6. TEG-Based Self-Powered Biosensors

As discussed earlier, the triboelectric layer can also modify chemically, with the aptamers and enzymes, and the same has been exploited to develop label-free, highly selective, and sensitive self-powered biosensors. In this section, we discuss some of the TEG-based active biological sensors.

6.1. Dopamine Sensors

Dopamine is a neurotransmitter that plays a crucial role in the central nervous system (CNS) and hormonal system.[159] Dopamine is a catecholamine, the abnormal levels associated

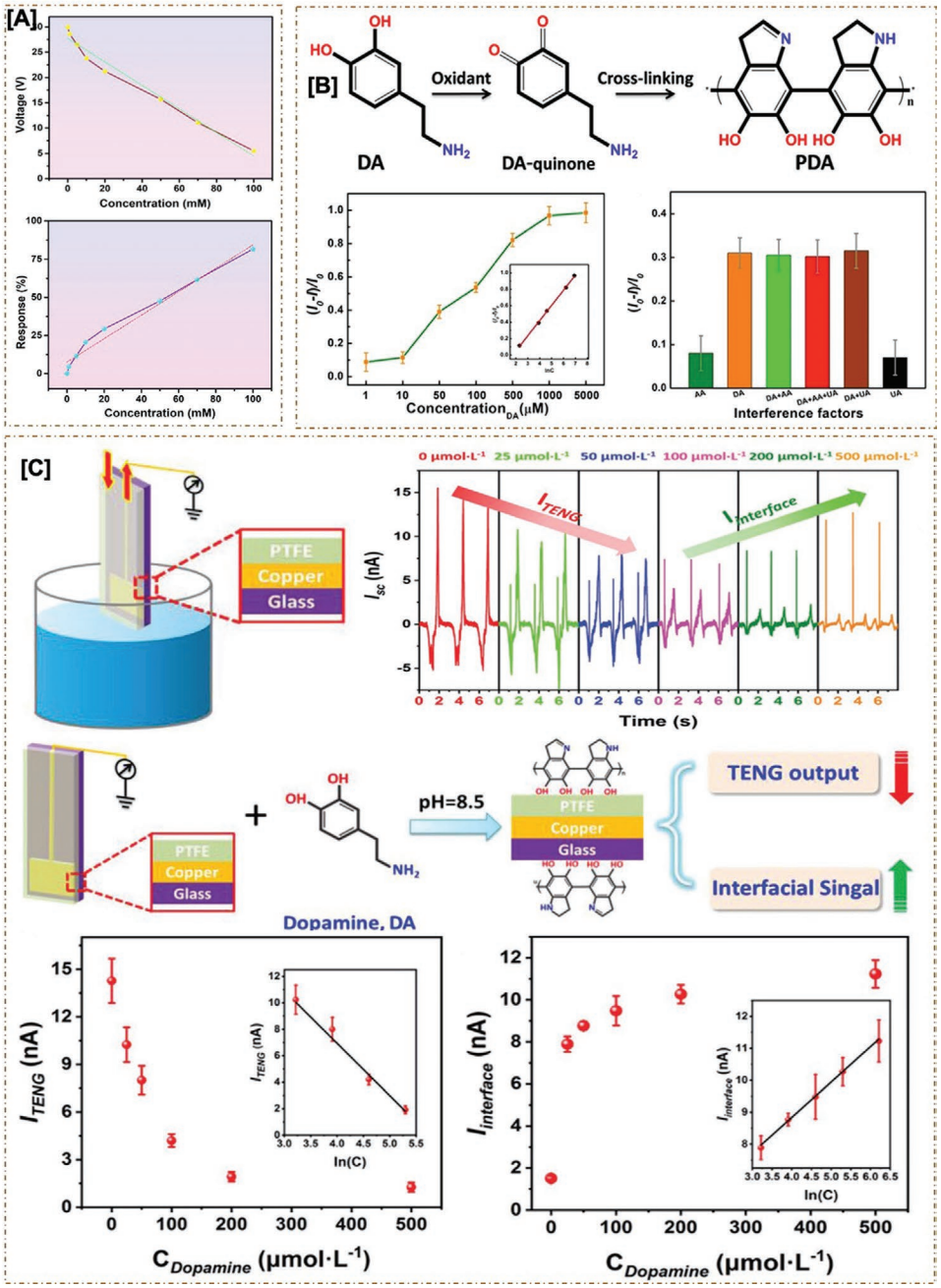

Figure 11. A) Voltage versus concentration and response profile of the cNF-TEG-based self-powered thioacetamide sensor. Reproduced with permission.[24] Copyright 2021, American Chemical Society. B) The oxidative self-polymerization of the dopamine to polydopamine. The short-circuit current ratio for different dopamine concentrations and sensors selectivity. Reproduced with permission.[30] Copyright 2015, American Chemical Society. C) Design of the liquid–solid TEG. The dopamine polymerization and its effect on the TEG and interfacial signal. The TEG and interfacial current versus dopamine concentrations (0–500 μmol L^{-1}). Reproduced with permission.[3a] Copyright 2019, Wiley-VCH.

with schizophrenia, Parkinson's disease, and Huntington's disease.[160] Several complicated and time-consuming techniques like high-performance liquid chromatography (HPLC), electrochemical methods and fluorescence spectrophotometry methods have been explored to detect dopamine.[160c,161] However, the existence of influencing analytes such as uric acid (UA) and ascorbic acids (AAs) make it challenging to use electrochemical methods for detection of dopamine.[161c,d,162] The issue could be addressed with TEG-based highly selective self-powered sensors such as the one based on nanostructured PTFE and aluminium as the contact layers.[30] The device generated an output of 116 V and 33 μA at 1 Hz, 60 N. The self-polymerization of dopamine to polydopamine (PDA) at basic pH is the key for the sensing. Figure 11B depicts the polymerization process of DA to PDA, which, when absorbed on the PTEF layer, can alter its surface potential and permittivity.[163]

Table 6. Comparison of TEG-based active liquid sensors.

Sensor	Negative TE layer	Positive TE layer	Range	Sensitivity	Ref.
Hg^{+2}	PDMS	Modified Au nanoparticles (NPs)	100×10^{-9} M to 5×10^{-6} M	–	[153]
Hg^{+2}	Acetone	Modified Au NPs	10×10^{-9} M to 1×10^{-6} M	–	[25]
Cu^{+2}, Pb^{+2} and Cr^{+3}	PTFE (NW)s	AAO nanopores	$0–200 \times 10^{-6}$ M	(Cu^{+2})—0.005 μM^{-1} (Pb^{+2})—0.003 μM^{-1} (Cr^{+3})—0.004 μM^{-1}	[154]
Phenol	PTFE	Modified TiO_2 (NW)	$10–100 \times 10^{-6}$ M	0.01 μM^{-1}	[26]
TAA	PTFE	Cu-Asp nanofibers	$1–100 \times 10^{-3}$ M	0.76 V mM^{-1}	[24]

Figure 11B also depicts the variation in the current ratio with the concentration of DA and interfering analytes, respectively. The results confirmed that the triboelectric nanosensor (TENS) is selective to dopamine.

Another example, of TEG-based DA sensors is based on solid–liquid single electrode.[3a] Figure 11C shows the schematic illustration of the device fabricated on a glass substrate with PTFE film as the active layer. The device generated two distinct signals: the conventional TEG signal due to triboelectrification and electrostatic induction. The second signal is due to the interfacial charges at the oil/water interface. Figure 11C illustrates the concept of the self-powered DA sensor which works on the principle of self-polymerization of DA to PDA at pH 8.5. The device exhibits the reduced TEG output and increased interfacial signal at different DA concentrations. The decreased TEG output is attributed to the PDA's low surface charges and better electrostatic screening. The increased interfacial signal observed due to the improved hydrophilicity contributes toward the enhanced electrostatic induction between the interfacial charges and the electrode. Figure 11C depicts the current output at different concentrations of DA. Figure 11C also shows the variation in the interfacial and TEG current signal with the concentration of the DA. The sensor showed good linearity in the concentration range of 25 to 250 μmol L^{-1}. The limit of detection (LOD) for the DA sensor was 3.96×10^{-6} and 5.15×10^{-6} M with $I_{Interface}$ and $I_{TEG,}$ respectively.

6.2. Catechin Sensors

Catechin has a polyphenol structure and is widely found in fruits, tea, chocolates, vegetables, and wine. It is beneficial as antioxidant, anti-microbial, anti-carcinogenic, radical scavenging, and anti-inflammation.[164] Further, it can also help reduce obesity, lowers glucose and plasma lipid levels.[164] Similar to DA, the techniques for catechin determination include HPLC, electrochemical and spectrophotometric methods. TEG-based catechin sensors are not explored much as we noted only one example reported so far.[165] **Figure 12**A illustrates the layered TEG structure comprising TiO_2 nanosheets (TNS) or TiO_2 NWs (TNW) as the bottom layer and PTFE as the top contact layer. The TNW-TEG produced an output voltage and current density of 4.3 V and 1.1 μA cm^{-2} respectively. Figure 12A shows the open-circuit voltage ratio in the presence of catechin for TNS-TEG and TNW-TEG, respectively. The TNW-TEG sensor showed a linear relationship in the range of $10–0.5 \times 10^{-3}$ M, while TNS-TEG exhibited a linear relationship ranging from 10×10^{-6} M to 0.25×10^{-3} M. The variation in the linear range is due to the high surface area of TNW, which results in the high absorption of catechin on the TNW array as confirmed experimentally.

6.3. Thrombin Sensors

Thrombin is an enzyme encoded by F2 gene and plays a vital role in regulating pathological and physiological processes. It is involved in the regulation of angiogenesis, tumour growth and metastasis.[166] Healthy individuals are characterized by the absence of thrombin in their blood.[167] The thrombin binding to aptamers is widely used for different immunoassays and clotting-based assays.[168] The aptamers are excellent bioreceptors as they offer good stability, sensitivity, and selectivity.[169] The conventional colorimetric and fluorometric thrombin sensor require labelling and are time-consuming. In addition, the electrochemical methods suffer from electrode fouling, poor detection limit, and stability. The TEG-based sensors, utilizing aptamer-protein interaction, can overcome the problems associated with conventional thrombin detection methods.[31] Figure 12B illustrates the concept of aptamer–protein-interaction-based TEG for thrombin detection. The TEG comprises Au nanoparticles (NPs) and PDMS active layers. The Au NPs offer a large contact area and can be easily modified with the anti-thrombin aptamer to provide high selectivity to the sensor. The anti-thrombin aptamers are negatively charged and can reduce the TEG output performance while interacting with the anti-thrombin. Figure 12B depicts the sensitivity of the sensor at different thrombin concentrations. The developed nanosensor showed a detection limit of 0.41×10^{-9} M (S/N = 3). The sensor exhibited an excellent selectivity for thrombin compared to the lysozyme and streptavidin. Moreover, a standalone sensor was demonstrated by lighting a different number of LEDs (6–17) depending on the concentration of thrombin. The bioreceptors or aptamers can also be replaced with other biomolecules to widen the scope for the label-free self-powered TEG sensing.

6.4. Creatinine Sensors

The creatinine (generated by breakdown of creatine phosphate) provides information on kidney functioning. High creatinine levels can be related to thyroid malfunction, muscular

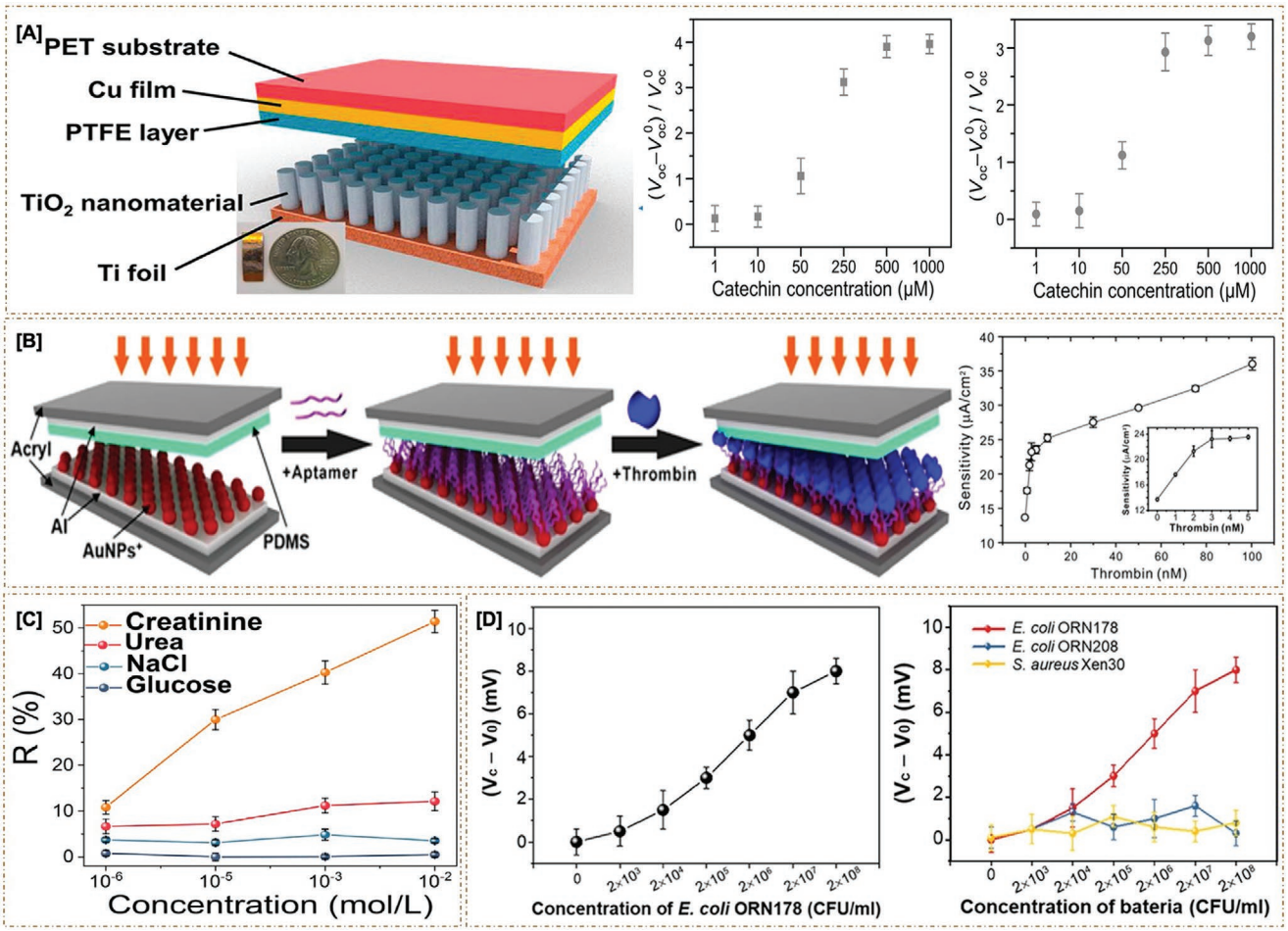

Figure 12. A) The self-powered TEG-based catechin sensor device design. The voltage ratio of TiO_2 (NW) and nanosheet-based catechin sensor. Reproduced with permission.[165] Copyright 2013, American Chemical Society. B) The DNA–aptamer-decorated Au nanoparticles based triboelectric biosensor for thrombin detection. The sensitivity of the sensor for different thrombin concentrations. Reproduced with permission.[31] Copyright 2016, Elsevier. C) The response of the sensor for the different analytes. Reproduced with permission.[3b] Copyright 2021, Elsevier. D) The voltage changes of the TENS for different ORN178 strain concentrations. The voltage changes of TENS for different bacterial strains at different concentrations. Reproduced with permission.[32] Copyright 2021, Elsevier.

disorders, and kidney issues.[170] The creatinine levels can also be used for diabetic neuropathy monitoring.[171] Just like previously discussed parameters, the creatinine is also be detected by the optical and chromatographic methods. However, the drawbacks (time intensive, complex operation, and expensive) of these conventional methods provide a room for creatinine detection via TEG.

A non-invasive, self-powered creatinine sensor based on enzyme-modified TEG was reported with PDMS and PANI serve as the negative and positive triboelectric layers.[3b] The enzymatic reaction produces H_2O_2, which can protonate the PANI. The PANI protonation alters its electrical conductivity and influences the TEG output. Figure 12C shows the response of the sensor for different molecules and based on limited data (e.g., four concentrations only) the sensor appears to be selective for the creatinine. The bending angle of the sensor also influences the device's performance. The sensor design is convenient for miniaturization, making it possible to integrate with traditional electronics and wearable devices. [3b]

6.5. Bacterial Detection

Bacteria are everywhere in nature, and many bacterial strains are pathogenic.[172] For example, *Escherichia coli* can cause diarrhoea, infections and its presence is also an indicator for environmental monitoring.[32] The conventional microbial detection methods like polymerase chain reaction (PCR), flow cytometry, fluorescence and electrochemical methods are complex, time-consuming and expensive with poor portability.[173] To address these issues, the TENS have been reported for detection of *E. coli*. As an example, a solid–liquid TENS based on the carbohydrate–protein interaction has been reported.[32] The modified Au NPs and phosphate buffer saline (PBS) are the solid and liquid interfaces in this device. The TENS probe, comprising D-mannose-functionalized Au NPs, is used to detect Concanavalin A (Con-A). The attachment of Con-A on the functionalized Au NPs reduces the work function of the layer from 6.72 eV to 5.32 eV. The reduced work function layer has a higher ability to transfer the electrons during contact electrification, thus enhancing the triboelectric output. The concept is then

utilized for *E. coli* detection. The type I pili of *E. coli* consists of many proteins. The *E. coli* strain ORN178 expresses FimH protein which has adhesion for the D-mannose. The other *E. coli* strains like ORN208 do not express FimH on its pili. When *E. coli* ORN178 was added to the PBS, it alters the surface potential as confirmed by the Kelvin probe force microscopy (KPFM). Figure 12D shows the change in the triboelectric output at different concentrations of the ORN178 strain. The variation confirms a linear sensing range of 10^4 to 10^7 CFU ml^{-1} with a LOD of 4×10^3 CFU ml^{-1}. Figure 12D depicts the sensor's selectivity in the presence of *E. coli* ORN208 and the *Staphylococcus aureus* XEN30 strain. The sensor was highly selective as other strains lack type I pili, resulting in the selective binding of the ORN178. The work is an excellent demonstration of the carbohydrate-protein interactions for self-powered label-free detection. Such interactions are inherent to many biological processes and can be utilized to develop selective healthcare sensors too.

6.6. Pharmacological Fingerprinting

The screening of large-scale drug candidate libraries requires high-throughput, cost-effective methods.[174] Conventional methods are unsuitable to meet the current pharmacological assessment demand for screening of new drugs. The cell lines can be used to record the cellular response to a drug molecule or any other chemical compound.[175]

A TEG-based non-invasive biosensing concept has been reported recently for cardiomyocytes.[33] The machine-learning algorithm was designed to study the signal variations. **Figure 13**A depicts the concept of the self-powered pharmacological assessment. The CPM-TEG comprises copper core and PDMS layer (Figure 13A). The mesh substrate is the core of the device for cardiomyocyte culture. The cardiac cells are made up of cardiac muscles, which are responsible for heart contraction. The contraction and relaxation of the cardiac cells can be used as a mechanical excitation for the TEG. The response of the

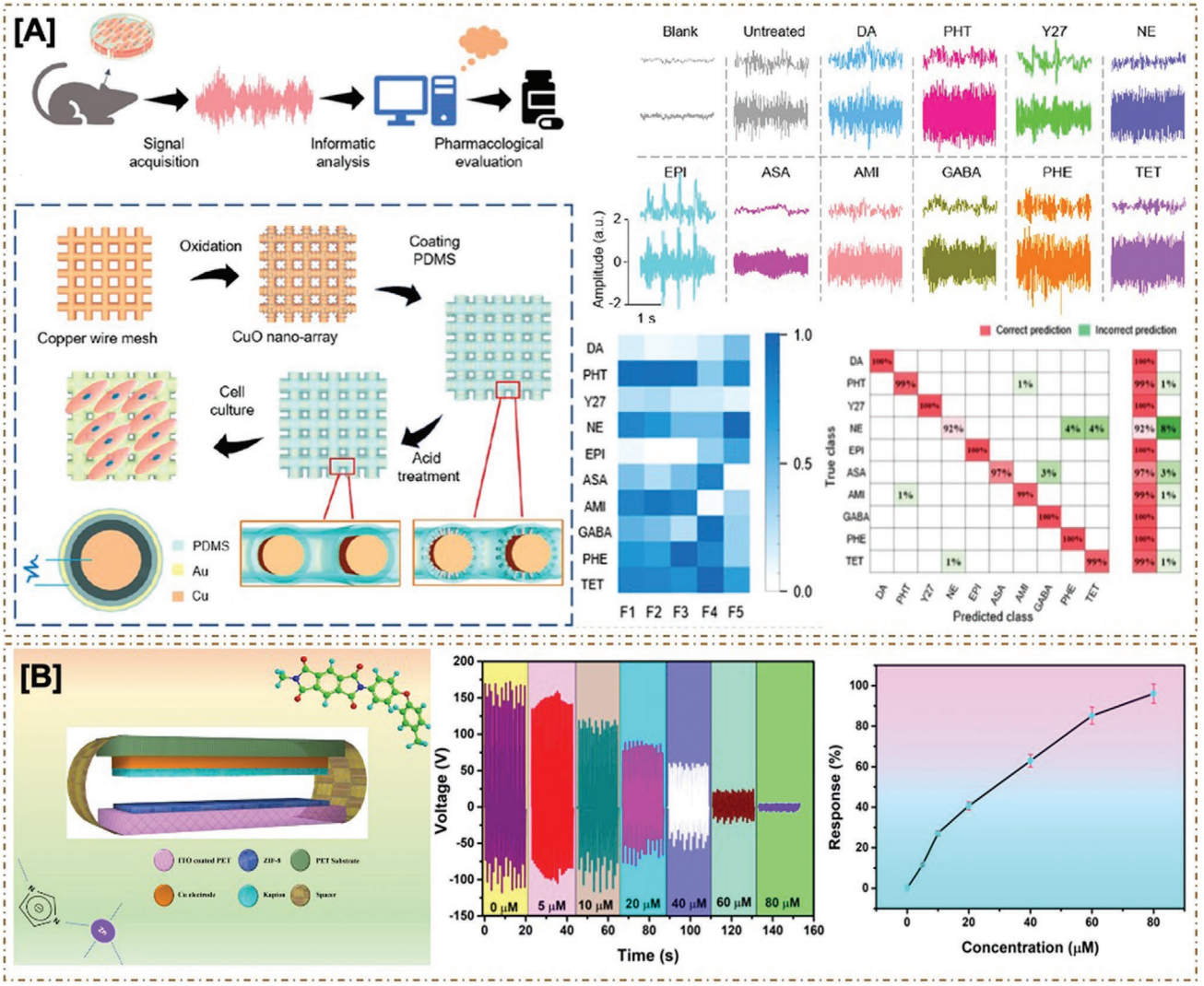

Figure 13. A) The concept and fabrication process of the CPM-TEG for pharmacological assessment. The signal from the CPM-TEG for 10 different drugs. The heat map and the confusion matrix for different drugs. Reproduced with permission.[33] Copyright 2020, American Chemical Society. B) 3D illustration of the ZIF-8-based MOF-TEG. The voltage and response of the MOF-TEG device for tetracycline sensing. Reproduced with permission.[5b] Copyright 2019, Wiley-VCH.

Table 7. Drugs and their effect on the cardiac cells.

Drug Name	Abbr.	Role	Ref.
Dopamine	DA	Helps in blood pressure and cardiac output	[176]
Norepinephrine	NE	Increases cardiac output	[177]
Epinephrine	EPI	Expands the coronary blood flow and improves the aortic diastolic pressure	[178]
Y-27632	Y27	Protects the heart	[179]
5,5-Diphenylhydantoin	PHT	Improves myocardial junction conduction, and in injured cardiac tissue, it shortens the duration of action potential	[180]
Acetylsalic Acid	ASA	Cardioprotective agent	[181]
γ-Aminobutyric acid	GABA	Decreases blood pressure and involve in the activation of γ-aminobutyric acid receptor to slow down the heart rate	[182]
Tetraethylthiuram disulfide	TET	Decreases systolic B.P and augment hypertension markers	[183]
Amitriptyline hydrochloride	AMI	Improves cardiac output	[184]
Phenacetin	PHE	Enhances hypertension and cardiovascular diseases	[185]

cardiomyocytes changes in the presence of drugs and can be used to predict the efficacy and identification of the drugs. The algorithm plays an important role in analysing and extract the features in a signal. The 10 drugs that are known to influence the cardiac cells were selected. The drugs and their effects are summarized in **Table 7**. Figure 13A shows the amplitude of the TEG output under blank, untreated and drug-treated conditions. The negligible signal in the case of blank confirms the prevention of the false positive detections. The algorithm then extracted two features in the temporal domain (F_1, F_2) and three features in the spectrum domain (F_3, F_4, F_5). Figure 13A also shows the heatmap of drugs signature obtained by the mean of the selected five features in the two domains. The drugs with similar effects on cardiomyocytes are close to each other in the score, for example, DA and EPI. Figure 13A depicts the validation performed on 10 drugs for the training and the testing sets. The support vector machine (SVM) was able to identify even the close drugs with an average accuracy of 98.5%. The use of TEG with machine learning to identify different drugs could be extended to a large drug library.[33] The informatic analysis is expected to play a major role in the development of TEG-based high-throughput drug screening systems.

6.7. Tetracycline Sensors

Tetracycline is a low-cost broad-spectrum antibiotic widely used for human healthcare to improve the efficacy of the feed, as animal medicine and foodstuff. The intensive use of antibiotics induces antibiotic resistance in the bacteria and render them more dangerous.[186] Additionally, the accumulation of tetracycline in humans can cause endocrine disorders and hearing loss.[187] A significant amount of tetracycline reaches the water bodies through different routes like faecal material and urine. The detection of tetracycline is important as its presence in water is dangerous for aquatic and human life. In this regard, TEG-based devices with a zeolitic imidazole framework (ZIF-8) MOF as the active layer has been explored recently.[5b] The TEG used ZIF-8 and Kapton as the active layers for the tetracycline sensing. Figure 13B shows a 3D image of the MOF-TEG along with the variation in the voltage and response of the sensor for different tetracycline concentrations. The tetracycline interacts with the ZIF-8 via π–π and electrostatic interactions. The voltage of MOF-TEG decreases with the tetracycline concentration due to the low electron density in the benzene ring of the tetracycline. The sensor was highly selective with a sensitivity of 3.12 V μM^{-1}. The excellence of the sensor lies in its reusability after a simple washing and drying process. For the first time, this work explored the multifunctional material MOF for energy harvesting via triboelectric effect. The high surface area, porosity, tuneable pore size and ease of post-synthetic modifications make the MOF an excellent material for self-powered sensors.

The evaluation of biocompatibility of sensors is essential for several applications, particularly the ones requiring in-vivo sensing. However, sensors discussed in this review are mainly used for the in-vitro detection of the analyte where biocompatibility is less critical. These TEG-based sensors were fabricated using materials like PTFE, TiO_2 nanostructures, PANI, PDMS and gold nanoparticles. The monolithic PTFE is considered as a biocompatible material but high-density PTFE (dPTFE) is not completely bioinert.[188] The dPTFE generated inflammatory macrophages and exhibited biocompatibility similar to that of collagen-based materials.[189] The TiO_2 nanostructures are biocompatible due to the presence of Ti–OH groups.[190] The gold nanoparticles are biocompatible in the concentration range of 5 mg mL^{-1}.[191] Similarly, PDMS also exhibits excellent biocompatibility.[192] Moreover, numerous TEGs based on natural materials like starch, plant leaves, cellulose, rice sheet, gelatin, silk fibroin and chitin are reported.[193] Natural materials offer excellent biodegradation in addition to biocompatibility. Apart from natural materials, synthetic polymers like polycaprolactone (PCL), poly(vinyl alcohol) (PVA), poly(hydroxy butyrate) (PHB), and poly(butylene adipate terephthalate) (PBAT) also offers biodegradation and biocompatibility. Furthermore, certain metal oxides (e.g., ZnO), silicone-based polymers (e.g., PDMS, Ecoflex), MOFs (e.g., MIL-88A), piezoelectrics (e.g., $BaTiO_3$), and 2D materials (e.g., graphene) are also biocompatible.[193] However, long-term influence of these materials on cells needs a detail analysis. A careful selection of materials is needed to develop a TEG that can offer exceptional biocompatibility. Although, there is a wide choice of biocompatible materials

but important consideration for in vivo biosensing is the device encapsulation, which must be an excellent biocompatible material. The encapsulated TEG-based biosensors are challenging as it makes it difficult for the analyte to reach the TEG active layer to influence the electrical performance of the device.

Multifunctional TEG-based biosensing is an interesting direction for future research. Lightweight, eco-friendly, low-cost multiparameter sensors powered by a sustainable and self-reliant source of energy are the strong attributes needed for healthcare, smart homes, and robotic applications.[194] It is challenging to attain these attributes and this is one reason why multi parameter chemical and biosensing using TEG has not been explored much. Multifunctional biosensors requirs a material that can distinguish two or multiple analytes while maintaining the high sensitivity and selectivity. In this regard, materials such as MOFs, peptides, hybrid nanomaterials are excellent candidates. In the case of TEGs, the growth of such materials on the conducting electrode could offer attractive options as active layer. The other approach is the use of polymer as a matrix with multifunctional materials incorporated as fillers. However, the use of polymer may reduce the porosity, which could hinder the direct interaction of analytes and may lead to devices having poor sensitivity and narrow detection range.

7. Applications of TEG-Based Active Chemical and Biosensors

The applications of mechanical, optical and magnetic sensors are not included here as they have been discussed in other review papers.[17,52a,105b,195] TEG-based chemical sensors and biosensors can be used for water-quality and air-quality monitoring, healthcare, and pharmaceuticals, as shown in **Figure 14**.

7.1. Water-Quality Monitoring

Water-quality monitoring is essential for the safety of the humans and the environment. The municipal and industrial waste water contains heavy metal ions (Pb, Hg, Cd, As etc.), antibiotics (tetracycline) and other chemicals (thioacetamide).[24,196] Heavy-metal ions even in trace levels can influence the cell signalling by interacting with the proteins. They can induce oxidative stress, inhibits the enzymes and metabolism, thus making their detection of utmost importance in the water.[196b] Similarly, its necessary to detect the antibiotics in the water as they can spread the antibiotic resistance. As discussed in previous sections, the TEG devices offer a simple, portable, selective and sensitive route for detection of heavy metal ions and antibiotics. Although still significant research is required to analyze the real-time sample with self-powered read out. The low-cost and simple design of TEG can soon lead to the development of self-powered disposable sensors for water-quality monitoring.

7.2. Air-Quality Monitoring

World Health Organization (WHO) data confirms the death of around 7 million people every year due to the air pollution. Almost the entire global population (≈ 90%) breathes air that has pollutant level higher than the WHO recommendations.[197] Air pollution not only causes harm to humans but also increases the threat to the climate. The TEG has been demonstrated for various contaminants including VOCs (benzene, phenol), gaseous pollutants (CO_2, H_2, NH_3, acetylene and aniline etc.).[26,119,121,129,133] TEGs have been proved to work in the low detection range (0–10 ppm), mid detection range (10–1000 ppm), and high detection range (100–10000 ppm), and hence they are excellent candidate for

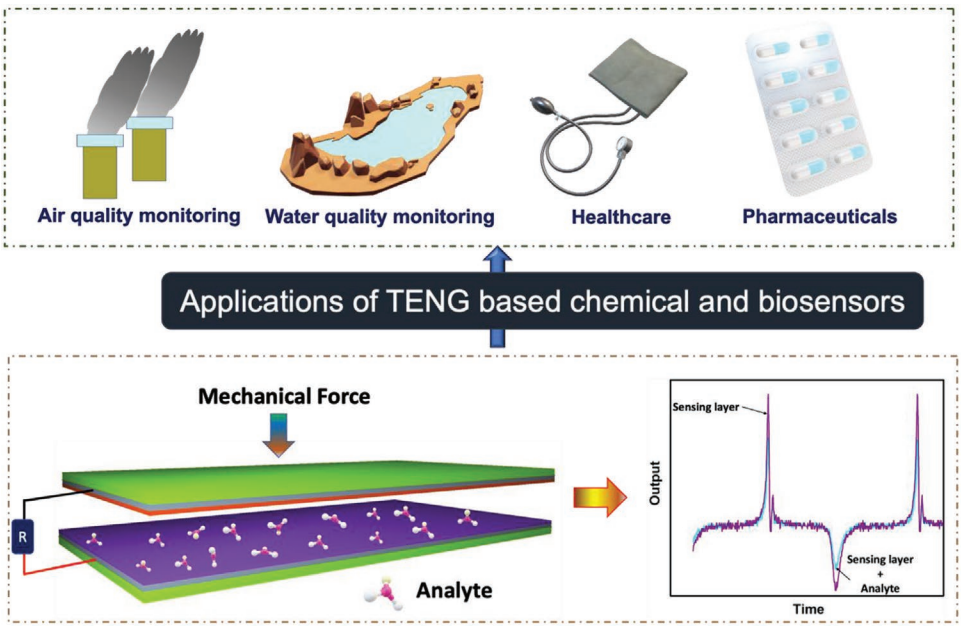

Figure 14. Mechanism and applications of TEG-based chemical and biosensors.

environment monitoring. They can add more value if they can be fabricated in different shapes as per the requirements of target applications. For example, a pipe shape triboelectric sensing unit has been developed for NO, CO and NH_3 sensing in the automotive exhaust pipe.[138] The TEG can be a future one stop solution for the environmental monitoring due to its wide working range, sensitivity and selectivity. However, much effort is still required in terms of device packaging to reduce the influence of the environmental factors like humidity and temperature.

7.3. Healthcare

The ability of the active layer to change its properties in the presence of an analyte makes the TEG suitable for the healthcare sensing, particularly for non-invasive systems integrated with wearables devices. The TEG has been demonstrated for the detection of different analytes like dopamine, creatinine, catechin, lactate and thrombin etc., the levels of which are associate with the diseases.[3b,30–31] Although TEGs have been able to detect the above analytes with good selectivity and sensitivity, analysis of real samples (e.g., real blood) is critical for proving the capabilities of TEGs for healthcare sensors. The ability to detect analytes in real samples in future can be a step toward the commercialization of TEG-based healthcare sensors.

7.4. Pharmaceuticals

The hidden ability of the TEG for pharmacological fingerprinting has been explored recently[33] by combining TEG response with machine learning algorithm to detect the effect of different drug treatments. The use of TEGs for pharmacological fingerprinting is new and yet to be explored further as it offers unique solution for high-throughput screening when combined with the machine learning. Such interesting data driven approaches could also advance the TEG sensing approach toward the newly emerging concept of internet of materials.

8. Summary, Challenges, and Future Perspective

TEGs are explored widely as direct sensors and power sources for numerous chemical and biosensors. The different device designs, materials, and mechanisms demonstrate the versatility of TEG in terms of detection of a wide variety of physical, chemical, and biological parameters. As discussed here, TEGs can be used for gas sensing, dopamine, catechin, tetracycline, thioacetamide, bacterial detection, and many more sensors,[3a,5b,24,32,121,165] and for the degradation of environmental contaminants.[26] TEG-based chemical and biosensors still need to be optimized to achieve the performance needed to replace conventional methods. Important factors (**Figure 15**) that can be considered for the development of such TEG sensors are explained below.

8.1. Sensitivity and Reliability

The detection capability of a sensor can be determined by a linear transfer function, the slope of which can provide their sensitivity. The general output characteristic curve in TEG-based sensors is between the output voltage or current and the concentration of the target molecule. Therefore, sensitivity is better when the change in the TEG device output is greater with the change in the concentration of the target molecule. The active layers with high charge densities are important for this purpose.[198] The TEG is highly influenced by environmental factors, altering the sensor sensitivity.[199] It is important to nullify the impact of these parameters or to use a controlled environment as an alternative for sensors. The TEG utilizes mechanical motions or vibrations, which can also influence the sensing measurements.[200] In the case of gas sensors, the flow of gas can give rise to an error by acting as a mechanical stimulus to the device. Such errors can be removed by carefully selecting the device substrate, using high impulse for the measurements, by mathematical compensation methods etc. The high sensitivity along with a wide detection range is an ideal scenario for any sensor. The detection range can also be related to the surface area of the sensing layer.[201] The response of TEG sensor depends on the absorbed analyte molecules. The poor

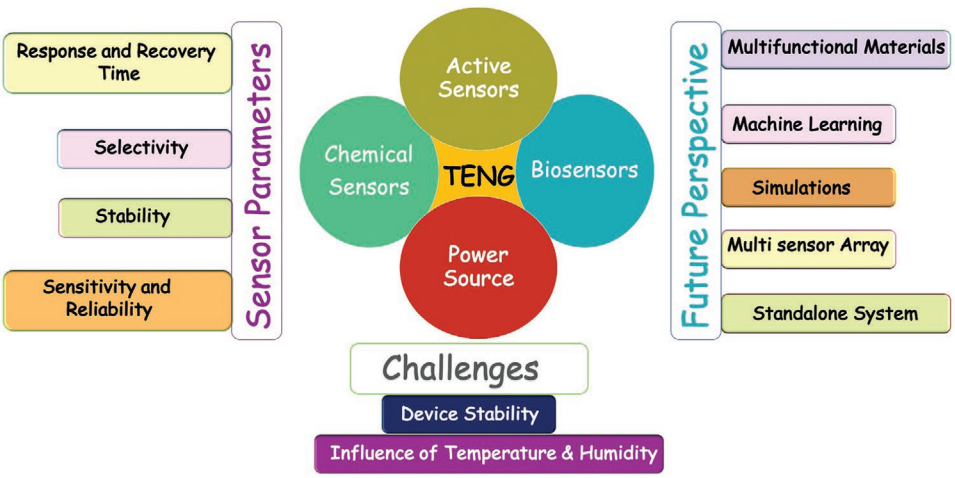

Figure 15. Sensor parameters, challenges, and future perspective of the self-powered chemical and biological sensors.

response at higher concentrations can be related to the occupancy of the available sites. The broad detection range thus can be obtained with the recognition elements with high surface area. The nano/microstructures, porous materials are useful in this aspect.[116a,154,202] The crystalline porous materials have attracted considerable interest as they can offer specific target sites, controlled porosity and high surface area.[5b,24,203] The high contact area will also improve the TEG output which is important to achieve the better sensitivity. The TEG can also act as a power source where the load matching dynamic range is important for the sensors.

8.2. Selectivity and Repeatability

Selectivity is vital for the accurate detection of the target parameter. The selective sensors exhibit poor responses to the interfering parameters or molecules. The selectivity can be achieved by the careful selection of the sensing materials. For example, ZIF-8-MOF-based devices are highly selective for detection of the tetracycline.[5b] Similarly, other highly selective sensors are discussed herein. The selectivity of the sensing layer can also be improved by doping, controlled porosity, chemical functionalization and modifications.[14a,15,204] Alternatively, the interfering molecules can be filtered out before passing the target molecule to the sensing layer.[205] Novel materials like MOFs, MXenes, and 2D materials will continue to play a major role in developing highly selective sensors.[5b,c,206] The repeatability is the ability of the sensor to provide same results on the identical samples measured under the same conditions.[207] The active-layer material, device design, and packaging are the factors that can influence the device repeatability.

8.3. Limit of Detection (LOD) and Limit of Quantification (LOQ)

The LOD is the lowest concentration of an analyte or substance that can be detected reliably by a sensor. Alternatively, the lowest concentration of an analyte or substance that shows a significant variation in the detected signal compare to the blank. Meanwhile the limit of quantification (LOQ) provides information on the lowest concentration that provides quantitatively meaningful measurements.[207–208]

8.4. Response and Recovery Time

The response time is the time taken by the sensor to achieve a value within ±10% of the value. at steady state. The recovery time is defined as the time taken by the sensor to reach its initial state after removing the measured variable. Faster response and recovery are desirable and important for practical applications. TEG-based gas sensors have showed high response and recovery time in most of the cases. The high recovery time is due to the time taken by the base air to replace the sample gas. A short response and recovery time are critical for the rapid detection of the varying concentration of the target molecule.

8.5. Stability

The stability of the sensing performance should not be affected by environmental and other factors. The stability of the TEG device or sensors is also related to the material of the active layer or the sensing layer. Materials like Teflon and Kapton are highly durable and can be used as the negative layer for TEG fabrication.[154,209] The sensing materials' mechanical stability, no influence of salt and other compounds on the sensing material are critical to achieve the reproducibility.[210] The stability of TEG against environmental factors can be achieved by packing the device and using mild conditions (force and frequency) for the measurements.[48b,211] The other important factor that can influence the device's stability is the ability of the material to return at the same position after removing the applied force. In this regard, highly elastic materials can be used as a spacer in the device.[212] The stable active sensing materials that are not influenced by the corrosive environment, mechanical force, humidity, and temperature are ideal for fabricating a stable sensor.

Efforts are required from the wider scientific community to address the challenges (Figure 15) for TEG-based sensors, so that they could offer real-time sensing. Firstly, the influence of environmental factors makes the device unreliable.[16] Continuous operation of the device after certain cycles induces wear and tear in the material.[213] The impact of environmental factors can be controlled to a certain extent by using a fully packed device and humidity-resistant materials.[48] The use of lubricant could also enhance the life of a TEG by reducing wear and tear.[213] However, the lubricant may not be suitable for the sensor, as it can interfere with the measurements. Secondly, there is a much greater need to design stand-alone systems with a self-powered readout. The TEGs produce discontinuous output and have high impedance and thus can only be used with power management circuits. The TEG's output is not sufficient to drive the complete sensor system with a readout circuit. While a few stand-alone TEG-based sensors have been demonstrated by turning LEDs on/off, the technique is suitable only to detect lowest and the highest concentrations. Further, machine-learning algorithms can be explored more to analyze or extract features from the obtained sensing signal. The algorithms are also important for big data analysis generated by the multisensor arrays. The multisensor arrays can be developed in the future to study multiple analytes at the same time. Simulations can also be used to select a stable, reliable, sensitive and selective sensing material. The emerging multifunctional materials such as MOFs are extremely important for chemical or biological detections[5b] as their composites (e.g., HKUST-1/PDMS) are stable under high humidity conditions.[48a] However, MOFs suffer from brittleness and it is tedious to grow them directly on the conducting materials or on flexible substrates, needed in applications such as wearable systems. In this regard, the printed electronics methods such as contact and transfer printing can offer interesting solutions,[214] potentially leading to a commercial sensor based on triboelectrification.

Acknowledgements

This work was supported in part by Engineering and Physical Science Research Council (EPSRC) through Engineering Fellowship (EP/R029644/1) and NextGenT-TEG Standard Grant (EP/V003380/1).

Conflict of Interest

The authors declare no conflict of interest.

Author Contributions

G.K. and R.D. conceptualized the idea. G.K wrote the original draft and R.D. reviewed and edited the manuscript. R.D. provided overall supervision.

Keywords

biosensors, chemical sensors, flexible electronics, self-powered sensors, triboelectric nanogenerators

Received: January 23, 2022
Revised: April 12, 2022
Published online: June 15, 2022

[1] a) M. Ghobakhloo, M. Fathi, M. Iranmanesh, P. Maroufkhani, M. E. Morales, *J. Cleaner Prod.* **2021**, *302*, 127052; b) R. Panchalingam, K. C. Chan, *Intell. Build. Int.* **2021**, *13*, 203; c) D. Elliott, W. Keen, L. Miao, *J. Traffic Transp. Eng.* **2019**, *6*, 109; d) E. S. Hosseini, S. Dervin, P. Ganguly, R. Dahiya, *ACS Appl. Bio Mater.* **2021**, *4*, 163; e) P. K. Murali, M. Kaboli, R. Dahiya, *Adv. Intell. Systems* **2021**, *4*, 2100122; f) R. Dahiya, N. Yogeswaran, F. Liu, L. Manjakkal, E. Burdet, V. Hayward, H. Jörntell, *Proc. IEEE* **2019**, *107*, 2016.

[2] a) R. Dahiya, D. Akinwande, J. S. Chang, *Proc. IEEE* **2019**, *107*, 2011; b) O. Ozioko, R. Dahiya, *Adv. Intell. Syst.* **2022**, *4*, 2100091; c) P. Karipoth, A. Christou, A. Pullanchiyodan, R. Dahiya, *Adv. Intell. Syst.* **2022**, *4*, 2100092; d) O. Ozioko, P. Karipoth, P. Escobedo, M. Ntagios, A. Pullanchiyodan, R. Dahiya, *Adv. Intell. Syst.* **2021**, *3*, 1900145; e) A. Christou, Y. Gao, W. T. Navaraj, H. Nassar, R. Dahiya, *Adv. Intell. Syst.* **2022**, *4*, 2000126.

[3] a) P. Jiang, L. Zhang, H. Guo, C. Chen, C. Wu, S. Zhang, Z. L. Wang, *Adv. Mater.* **2019**, *31*, 1902793; b) Y. Luo, T. Zhao, Y. Dai, Q. Li, H. Fu, *Sens. Actuators, A* **2021**, *320*, 112585; c) N. S. Oliver, C. Toumazou, A. E. G. Cass, D. G. Johnston, *Diabetic Med.* **2009**, *26*, 197; d) S. Dervin, P. Ganguly, R. Dahiya, *IEEE Sens. J.* **2021**, *21*, 26226; e) M. A. Kafi, A. Paul, A. Vilouras, E. S. Hosseini, R. S. Dahiya, *IEEE Sens. J.* **2020**, *20*, 6794; f) A. Vilouras, R. Dahiya, in *2021 IEEE Int. Symp. on Circuits and Systems (ISCAS)*, IEEE, Piscataway, NJ, USA **2021**, https://doi.org/10.1109/ISCAS51556.2021.9401616.

[4] a) M. Bhattacharjee, A. Vilouras, R. Dahiya, in *2019 IEEE Int. Conf. on Flexible and Printable Sensors and Systems (FLEPS)*, IEEE, Piscataway, NJ, USA **2019**, https://doi.org/10.1109/FLEPS.2019.8792237; b) H. Karimi-Maleh, Y. Orooji, F. Karimi, M. Alizadeh, M. Baghayeri, J. Rouhi, S. Tajik, H. Beitollahi, S. Agarwal, V. K. Gupta, S. Rajendran, A. Ayati, L. Fu, A. L. Sanati, B. Tanhaei, F. Sen, M. shabani-nooshabadi, P. N. Asrami, A. Al-Othman, *Biosens. Bioelectron.* **2021**, *184*, 113252; c) C. Chen, J. Wang, *Analyst* **2020**, *145*, 1605; d) L. Manjakkal, S. Mitra, Y. Petillo, J. Shutler, M. Scott, M. Willander, R. Dahiya, *IEEE Internet Things J.* **2021**, *8*, 13805; e) M. Bhattacharjee, M. Soni, P. Escobedo, R. Dahiya, *Adv. Electron. Mater.* **2020**, *6*, 2000445; f) A. Vilouras, A. Christou, L. Manjakkal, R. Dahiya, *ACS Appl. Electron. Mater.* **2020**, *2*, 2601; g) E. S. Hosseini, L. Manjakkal, D. Shakthivel, R. Dahiya, *ACS Appl. Mater. Interfaces* **2020**, *12*, 9008.

[5] a) G. Khandelwal, N. P. Maria Joseph Raj, S.-J. Kim, *Adv. Energy Mater.* **2021**, *11*, 2101170; b) G. Khandelwal, A. Chandrasekhar, N. P. Maria Joseph Raj, S.-J. Kim, *Adv. Energy Mater.* **2019**, *9*, 1803581; c) M. Seol, S. Kim, Y. Cho, K.-E. Byun, H. Kim, J. Kim, S. K. Kim, S.-W. Kim, H.-J. Shin, S. Park, *Adv. Mater.* **2018**, *30*, 1801210; d) V. Schroeder, S. Savagatrup, M. He, S. Lin, T. M. Swager, *Chem. Rev.* **2019**, *119*, 599; e) M. M. Rahman, A. Jamal, S. B. Khan, M. Faisal, *Biosens. Bioelectron.* **2011**, *28*, 127.

[6] a) M. Li, S. K. Cushing, N. Wu, *Analyst* **2015**, *140*, 386; b) S. Mross, S. Pierrat, T. Zimmermann, M. Kraft, *Biosens. Bioelectron.* **2015**, *70*, 376; c) E. Bakker, M. Telting-Diaz, *Anal. Chem.* **2002**, *74*, 2781; d) P. Skládal, *TrAC Trends Anal. Chem.* **2016**, *79*, 127; e) P. Escobedo, M. Bhattacharjee, F. Nikbakhtnasrabadi, R. Dahiya, *IEEE Sens. J.* **2021**, *21*, 26406; f) F. Nikbakhtnasrabadi, H. El Matbouly, M. Ntagios, R. Dahiya, *ACS Appl. Electron. Mater.* **2021**, *3*, 2233; g) P. Escobedo, M. Bhattacharjee, F. Nikbakhtnasrabadi, R. Dahiya, *IEEE Internet Things J.* **2021**, *8*, 5093; h) M. Bhattacharjee, F. Nikbakhtnasrabadi, R. Dahiya, *IEEE Internet Things J.* **2021**, *8*, 5101; i) N. Yogeswaran, E. S. Hosseini, R. Dahiya, *ACS Appl. Mater. Interfaces* **2020**, *12*, 54035; j) M. Shojaei Baghini, A. Vilouras, M. Douthwaite, P. Georgiou, R. Dahiya, *Electrochem. Sci. Adv.* **2021**, https://doi.org/10.1002/elsa.202100202; k) Q. Zhou, J. Pan, S. Deng, F. Xia, T. Kim, *Adv. Mater.* **2021**, *33*, 2008276.

[7] a) S. Stauss, I. Honma, *Bull. Chem. Soc. Jpn.* **2018**, *91*, 492; b) L. Manjakkal, L. Yin, A. Nathan, J. Wang, R. Dahiya, *Adv. Mater.* **2021**, *33*, 2100899; c) P. Forouzandeh, P. Ganguly, R. Dahiya, S. C. Pillai, *J. Power Sources* **2022**, *519*, 230744; d) R. Mukherjee, P. Ganguly, R. Dahiya, *Adv. Intell. Syst.* **2021**, https://doi.org/10.1002/aisy.202100036.

[8] a) L. Manjakkal, W. T. Navaraj, C. G. Núñez, R. Dahiya, *Adv. Sci.* **2019**, *6*, 1802251; b) A. Pullanchiyodan, L. Manjakkal, M. Ntagios, R. Dahiya, *ACS Appl. Mater. Interfaces* **2021**, *13*, 47581.

[9] a) C. García Núñez, L. Manjakkal, R. Dahiya, *npj Flexible Electron.* **2019**, *3*, 1; b) G. Min, A. Pullanchiyodan, A. S. Dahiya, E. S. Hosseini, Y. Xu, D. M. Mulvihill, R. Dahiya, *Nano Energy* **2021**, *90*, 106600.

[10] Y. Xu, G. Min, N. Gadegaard, R. Dahiya, D. M. Mulvihill, *Nano Energy* **2020**, *76*, 105067.

[11] P. Escobedo, M. Ntagios, D. Shakthivel, W. T. Navaraj, R. Dahiya, *IEEE Trans. Rob.* **2021**, *37*, 683.

[12] F.-R. Fan, Z.-Q. Tian, Z. L. Wang, *Nano Energy* **2012**, *1*, 328.

[13] D. W. Kim, J. H. Lee, J. K. Kim, U. Jeong, *NPG Asia Mater.* **2020**, *12*, 6.

[14] a) Y. Liu, J. Mo, Q. Fu, Y. Lu, N. Zhang, S. Wang, S. Nie, *Adv. Funct. Mater.* **2020**, *30*, 2004714; b) S. Li, Y. Fan, H. Chen, J. Nie, Y. Liang, X. Tao, J. Zhang, X. Chen, E. Fu, Z. L. Wang, *Energy Environ. Sci.* **2020**, *13*, 896; c) M.-L. Seol, J.-H. Woo, D.-I. Lee, H. Im, J. Hur, Y.-K. Choi, *Small* **2014**, *10*, 3887.

[15] C. Huang, G. Chen, A. Nashalian, J. Chen, *Nanoscale* **2021**, *13*, 2065.

[16] V. Nguyen, R. Yang, *Nano Energy* **2013**, *2*, 604.

[17] Q. Gao, T. Cheng, Z. L. Wang, *Extreme Mech. Lett.* **2021**, *42*, 101100.

[18] Y. S. Zhou, G. Zhu, S. Niu, Y. Liu, P. Bai, Q. Jing, Z. L. Wang, *Adv. Mater.* **2014**, *26*, 1719.

[19] Q. Han, Z. Ding, Z. Qin, T. Wang, X. Xu, F. Chu, *Nano Energy* **2020**, *67*, 104277.

[20] B. Zhang, L. Zhang, W. Deng, L. Jin, F. Chun, H. Pan, B. Gu, H. Zhang, Z. Lv, W. Yang, Z. L. Wang, *ACS Nano* **2017**, *11*, 7440.

[21] T. Li, J. Zou, F. Xing, M. Zhang, X. Cao, N. Wang, Z. L. Wang, *ACS Nano* **2017**, *11*, 3950.

[22] P. Bai, G. Zhu, Q. Jing, J. Yang, J. Chen, Y. Su, J. Ma, G. Zhang, Z. L. Wang, *Adv. Funct. Mater.* **2014**, *24*, 5807.
[23] Y. Su, J. Wang, B. Wang, T. Yang, B. Yang, G. Xie, Y. Zhou, S. Zhang, H. Tai, Z. Cai, G. Chen, Y. Jiang, L.-Q. Chen, J. Chen, *ACS Nano* **2020**, *14*, 6067.
[24] G. Khandelwal, M. K. Ediriweera, N. Kumari, N. P. Maria Joseph Raj, S. K. Cho, S.-J. Kim, *ACS Appl. Mater. Interfaces* **2021**, *13*, 18887.
[25] A. Pal, S. Chatterjee, S. Saha, S. R. Barman, D. Choi, S. Lee, Z.-H. Lin, *ECS J. Solid State Sci. Technol.* **2020**, *9*, 115029.
[26] Z. Li, J. Chen, J. Yang, Y. Su, X. Fan, Y. Wu, C. Yu, Z. L. Wang, *Energy Environ. Sci.* **2015**, *8*, 887.
[27] H. Zhang, Y. Yang, Y. Su, J. Chen, C. Hu, Z. Wu, Y. Liu, C. P. Wong, Y. Bando, Z. L. Wang, *Nano Energy* **2013**, *2*, 693.
[28] S. Qi, H. Guo, J. Chen, J. Fu, C. Hu, M. Yu, Z. L. Wang, *Nanoscale* **2018**, *10*, 4745.
[29] L. Su, Z. X. Zhao, H. Y. Li, J. Yuan, Z. L. Wang, G. Z. Cao, G. Zhu, *ACS Nano* **2015**, *9*, 11310.
[30] Y. Jie, N. Wang, X. Cao, Y. Xu, T. Li, X. Zhang, Z. L. Wang, *ACS Nano* **2015**, *9*, 8376.
[31] Y. K. Jung, K. N. Kim, J. M. Baik, B.-S. Kim, *Nano Energy* **2016**, *30*, 77.
[32] Y.-P. Pao, C.-C. Yu, Y.-Z. Lin, S. Chatterjee, S. Saha, N. Tiwari, Y.-T. Huang, C.-C. Wu, D. Choi, Z.-H. Lin, *Nano Energy* **2021**, *85*, 106008.
[33] X. Ji, P. Fang, B. Xu, K. Xie, H. Yue, X. Luo, Z. Wang, X. Zhao, P. Shi, *Nano Lett.* **2020**, *20*, 4043.
[34] a) Z. L. Wang, J. Song, *Science* **2006**, *312*, 242; b) M. Ma, Z. Kang, Q. Liao, Q. Zhang, F. Gao, X. Zhao, Z. Zhang, Y. Zhang, *Nano Res.* **2018**, *11*, 2951; c) R. Hiptmair, *Acta Numerica* **2002**, *11*, 237; d) Z. L. Wang, *Mater. Today* **2017**, *20*, 74.
[35] W. J. Kim, V. Vivekananthan, G. Khandelwal, A. Chandrasekhar, S.-J. Kim, *ACS Appl. Electron. Mater.* **2020**, *2*, 3100.
[36] a) V. Vivekananthan, A. Chandrasekhar, N. R. Alluri, Y. Purusothaman, G. Khandelwal, R. Pandey, S.-J. Kim, *Nano Energy* **2019**, *64*, 103926; b) X. Fan, J. He, J. Mu, J. Qian, N. Zhang, C. Yang, X. Hou, W. Geng, X. Wang, X. Chou, *Nano Energy* **2020**, *68*, 104319.
[37] J. C. Maxwell, *London, Edinburgh Dublin Philos. Mag. J. Sci., Ser. 4* **1861**, *21*, 161.
[38] a) G. Stewart, D. Gallai, *Science Scope, ProQuest* **1998**, *21*, 18; b) J. Moser, *London, Edinburgh, Dublin Philos. Mag. J. Sci.* **1881**, *12*, 130.
[39] M. B. Ege, A. Font, S. Bolat, O. Kalenderli, in *2014 ICHVE Int. Conf. on High Voltage Engineering and Application*, IEEE, PIscataway, NJ, USA **2014**, https://doi.org/10.1109/ICHVE.2014.7035497.
[40] F. A. Furfari, *IEEE Industry Appl. Mag.* **2005**, *11*, 10.
[41] Z. L. Wang, A. C. Wang, *Mater. Today* **2019**, *30*, 34.
[42] M. Sun, Q. Lu, Z. L. Wang, B. Huang, *Nat. Commun.* **2021**, *12*, 1752.
[43] S. Chatterjee, S. R. Burman, I. Khan, S. Saha, D. Choi, S. Lee, Z.-H. Lin, *Nanoscale* **2020**, *12*, 17663.
[44] a) S. Niu, Y. Liu, S. Wang, L. Lin, Y. S. Zhou, Y. Hu, Z. L. Wang, *Adv. Mater.* **2013**, *25*, 6184; b) S. Niu, S. Wang, L. Lin, Y. Liu, Y. S. Zhou, Y. Hu, Z. L. Wang, *Energy Environ. Sci.* **2013**, *6*, 3576; c) Z. L. Wang, *ACS Nano* **2013**, *7*, 9533.
[45] Y. Zi, S. Niu, J. Wang, Z. Wen, W. Tang, Z. L. Wang, *Nat. Commun.* **2015**, *6*, 8376.
[46] Z. L. Wang, *Faraday Discuss.* **2014**, *176*, 447.
[47] C. X. Lu, C. B. Han, G. Q. Gu, J. Chen, Z. W. Yang, T. Jiang, C. He, Z. L. Wang, *Adv. Eng. Mater.* **2017**, *19*, 1700275.
[48] a) R. Wen, J. Guo, A. Yu, J. Zhai, Z. l. Wang, *Adv. Funct. Mater.* **2019**, *29*, 1807655; b) A. Chandrasekhar, V. Vivekananthan, G. Khandelwal, S. J. Kim, *Nano Energy* **2019**, *60*, 850.
[49] M. S. Mannoor, H. Tao, J. D. Clayton, A. Sengupta, D. L. Kaplan, R. R. Naik, N. Verma, F. G. Omenetto, M. C. McAlpine, *Nat. Commun.* **2012**, *3*, 763.
[50] a) Q. Miao, C. Liu, N. Zhang, K. Lu, H. Gu, J. Jiao, J. Zhang, Z. Wang, X. Zhou, *ACS Appl. Electron. Mater.* **2020**, *2*, 3072; b) H. Lei, Y. Chen, Z. Gao, Z. Wen, X. Sun, *J. Mater. Chem. A* **2021**, *9*, 20100; c) D. Zhang, D. Wang, Z. Xu, X. Zhang, Y. Yang, J. Guo, B. Zhang, W. Zhao, *Coord. Chem. Rev.* **2021**, *427*, 213597; d) J. Tao, R. Bao, X. Wang, Y. Peng, J. Li, S. Fu, C. Pan, Z. L. Wang, *Adv. Funct. Mater.* **2019**, *29*, 1806379.
[51] a) M. R. Cutkosky, R. D. Howe, W. R. Provancher, in *Springer Handbook of Robotics* (Eds: B. Siciliano, O. Khatib), Springer, Berlin/Heidelberg, Germany **2008**, p. 455; b) Y. Al-Handarish, O. M. Omisore, T. Igbe, S. Han, H. Li, W. Du, J. Zhang, L. Wang, *Adv. Mater. Sci. Eng.* **2020**, *2020*, 4047937.
[52] a) E. Hwang, J. Seo, Y. Kim, *J. Microelectromech. Syst.* **2007**, *16*, 556; b) L. Zou, C. Ge, Z. J. Wang, E. Cretu, X. Li, *Sensors* **2017**, *17*, 2653.
[53] J. Luo, W. Gao, Z. L. Wang, *Adv. Mater.* **2021**, *33*, 2004178.
[54] Z. Zhou, X. Li, Y. Wu, H. Zhang, Z. Lin, K. Meng, Z. Lin, Q. He, C. Sun, J. Yang, Z. L. Wang, *Nano Energy* **2018**, *53*, 501.
[55] C. Zhang, J. Chen, W. Xuan, S. Huang, L. Shi, Z. Cao, Z. Ye, Y. Li, X. Wang, S. Dong, A. J. Flewitt, H. Jin, J. Luo, *Nano Energy* **2022**, *92*, 106770.
[56] Z. Lin, J. Chen, X. Li, Z. Zhou, K. Meng, W. Wei, J. Yang, Z. L. Wang, *ACS Nano* **2017**, *11*, 8830.
[57] Y. Zou, P. Tan, B. Shi, H. Ouyang, D. Jiang, Z. Liu, H. Li, M. Yu, C. Wang, X. Qu, L. Zhao, Y. Fan, Z. L. Wang, Z. Li, *Nat. Commun.* **2019**, *10*, 2695.
[58] M. Chen, X. Li, L. Lin, W. Du, X. Han, J. Zhu, C. Pan, Z. L. Wang, *Adv. Funct. Mater.* **2014**, *24*, 5059.
[59] W. Li, G. Liu, D. Jiang, C. Wang, W. Li, T. Guo, J. Zhao, F. Xi, W. Liu, C. Zhang, *Adv. Mater. Technol.* **2018**, *3*, 1800189.
[60] Q. Jing, Y. S. Choi, M. Smith, N. Ćatić, C. Ou, S. Kar-Narayan, *Adv. Mater. Technol.* **2019**, *4*, 1800328.
[61] C. P. Vo, M. Shahriar, C. D. Le, K. K. Ahn, *Int. J. Precision Eng. Manuf.-Green Technol.* **2019**, *6*, 741.
[62] Z. Xie, J. Dong, F. Yang, R. Xu, Q. Gao, T. Cheng, Z. L. Wang, *Extreme Mech. Lett.* **2020**, *37*, 100713.
[63] Y. Wu, Q. Jing, J. Chen, P. Bai, J. Bai, G. Zhu, Y. Su, Z. L. Wang, *Adv. Funct. Mater.* **2015**, *25*, 2166.
[64] X. S. Meng, H. Y. Li, G. Zhu, Z. L. Wang, *Nano Energy* **2015**, *12*, 606.
[65] X. H. Li, C. B. Han, T. Jiang, C. Zhang, Z. L. Wang, *Nanotechnology* **2016**, *27*, 085401.
[66] X. Pu, H. Guo, Q. Tang, J. Chen, L. Feng, G. Liu, X. Wang, Y. Xi, C. Hu, Z. L. Wang, *Nano Energy* **2018**, *54*, 453.
[67] C. He, B. D. Chen, T. Jiang, L. Xu, C. B. Han, G. Q. Gu, Z. L. Wang, *Adv. Mater. Technol.* **2018**, *3*, 1700251.
[68] Z. Wang, J. An, J. Nie, J. Luo, J. Shao, T. Jiang, B. Chen, W. Tang, Z. L. Wang, *Adv. Mater.* **2020**, *32*, 2001466.
[69] Z. Xie, J. Dong, Y. Li, L. Gu, B. Song, T. Cheng, Z. L. Wang, *Extreme Mech. Lett.* **2020**, *34*, 100595.
[70] Y. Yang, H. Zhang, J. Chen, Q. Jing, Y. S. Zhou, X. Wen, Z. L. Wang, *ACS Nano* **2013**, *7*, 7342.
[71] C. B. Han, C. Zhang, X. H. Li, L. Zhang, T. Zhou, W. Hu, Z. L. Wang, *Nano Energy* **2014**, *9*, 325.
[72] Q. Jing, G. Zhu, W. Wu, P. Bai, Y. Xie, R. P. S. Han, Z. L. Wang, *Nano Energy* **2014**, *10*, 305.
[73] H. Zhang, Y. Yang, Y. Su, J. Chen, K. Adams, S. Lee, C. Hu, Z. L. Wang, *Adv. Funct. Mater.* **2014**, *24*, 1401.
[74] F. Yi, L. Lin, S. Niu, J. Yang, W. Wu, S. Wang, Q. Liao, Y. Zhang, Z. L. Wang, *Adv. Funct. Mater.* **2014**, *24*, 7488.
[75] Y. K. Pang, X. H. Li, M. X. Chen, C. B. Han, C. Zhang, Z. L. Wang, *ACS Appl. Mater. Interfaces* **2015**, *7*, 19076.

[76] Y. Hu, J. Yang, Q. Jing, S. Niu, W. Wu, Z. L. Wang, *ACS Nano* **2013**, *7*, 10424.
[77] J. Chen, G. Zhu, W. Yang, Q. Jing, P. Bai, Y. Yang, T.-C. Hou, Z. L. Wang, *Adv. Mater.* **2013**, *25*, 6094.
[78] S. Wang, S. Niu, J. Yang, L. Lin, Z. L. Wang, *ACS Nano* **2014**, *8*, 12004.
[79] J. Zhu, X. Hou, X. Niu, X. Guo, J. Zhang, J. He, T. Guo, X. Chou, C. Xue, W. Zhang, *Sens. Actuators, A* **2017**, *263*, 317.
[80] H. Yu, X. He, W. Ding, Y. Hu, D. Yang, S. Lu, C. Wu, H. Zou, R. Liu, C. Lu, Z. L. Wang, *Adv. Energy Mater.* **2017**, *7*, 1700565.
[81] Y. Chen, Y.-C. Wang, Y. Zhang, H. Zou, Z. Lin, G. Zhang, C. Zou, Z. L. Wang, *Adv. Energy Mater.* **2018**, *8*, 1802159.
[82] H. Guo, X. Jia, L. Liu, X. Cao, N. Wang, Z. L. Wang, *ACS Nano* **2018**, *12*, 3461.
[83] M. Xu, P. Wang, Y.-C. Wang, S. L. Zhang, A. C. Wang, C. Zhang, Z. Wang, X. Pan, Z. L. Wang, *Adv. Energy Mater.* **2018**, *8*, 1702432.
[84] Q. Shi, H. Wang, T. He, C. Lee, in *2018 IEEE 13th Annu. Int. Conf. on Nano/Micro Engineered and Molecular Systems (NEMS)*, IEEE, Piscataway, NJ, USA **2018**, pp. 487–490.
[85] Q. He, Y. Wu, Z. Feng, C. Sun, W. Fan, Z. Zhou, K. Meng, E. Fan, J. Yang, *Nano Energy* **2019**, *59*, 689.
[86] J. Chen, H. Guo, Z. Wu, G. Xu, Y. Zi, C. Hu, Z. L. Wang, *Nano Energy* **2019**, *64*, 103920.
[87] C. Liu, Y. Wang, N. Zhang, X. Yang, Z. Wang, L. Zhao, W. Yang, L. Dong, L. Che, G. Wang, X. Zhou, *Nano Energy* **2020**, *67*, 104228.
[88] P.-K. Yang, Z.-H. Lin, K. C. Pradel, L. Lin, X. Li, X. Wen, J.-H. He, Z. L. Wang, *ACS Nano* **2015**, *9*, 901.
[89] Z. Liu, Y. Ma, H. Ouyang, B. Shi, N. Li, D. Jiang, F. Xie, D. Qu, Y. Zou, Y. Huang, H. Li, C. Zhao, P. Tan, M. Yu, Y. Fan, H. Zhang, Z. L. Wang, Z. Li, *Adv. Funct. Mater.* **2019**, *29*, 1807560.
[90] K. Dong, Z. Wu, J. Deng, A. C. Wang, H. Zou, C. Chen, D. Hu, B. Gu, B. Sun, Z. L. Wang, *Adv. Mater.* **2018**, *30*, 1804944.
[91] T. Chen, M. Zhao, Q. Shi, Z. Yang, H. Liu, L. Sun, J. Ouyang, C. Lee, *Nano Energy* **2018**, *51*, 162.
[92] Y. Yang, H. Zhang, Z.-H. Lin, Y. S. Zhou, Q. Jing, Y. Su, J. Yang, J. Chen, C. Hu, Z. L. Wang, *ACS Nano* **2013**, *7*, 9213.
[93] L. Lin, Y. Xie, S. Wang, W. Wu, S. Niu, X. Wen, Z. L. Wang, *ACS Nano* **2013**, *7*, 8266.
[94] G. Zhu, W. Q. Yang, T. Zhang, Q. Jing, J. Chen, Y. S. Zhou, P. Bai, Z. L. Wang, *Nano Lett.* **2014**, *14*, 3208.
[95] X.-Z. Jiang, Y.-J. Sun, Z. Fan, T.-Y. Zhang, *ACS Nano* **2016**, *10*, 7696.
[96] X. Wang, H. Zhang, L. Dong, X. Han, W. Du, J. Zhai, C. Pan, Z. L. Wang, *Adv. Mater.* **2016**, *28*, 2896.
[97] X. Pu, M. Liu, X. Chen, J. Sun, C. Du, Y. Zhang, J. Zhai, W. Hu, Z. L. Wang, *Sci. Adv.* **2017**, *3*, 1700015.
[98] X. X. Zhu, Z. B. Li, X. S. Li, L. Su, X. Y. Wei, S. Y. Kuang, B. W. Su, J. Yang, Z. L. Wang, G. Zhu, *Nano Energy* **2018**, *50*, 497.
[99] Z. Ren, J. Nie, J. Shao, Q. Lai, L. Wang, J. Chen, X. Chen, Z. L. Wang, *Adv. Funct. Mater.* **2018**, *28*, 1802989.
[100] G. Zhao, Y. Zhang, N. Shi, Z. Liu, X. Zhang, M. Wu, C. Pan, H. Liu, L. Li, Z. L. Wang, *Nano Energy* **2019**, *59*, 302.
[101] K. Zhou, Y. Zhao, X. Sun, Z. Yuan, G. Zheng, K. Dai, L. Mi, C. Pan, C. Liu, C. Shen, *Nano Energy* **2020**, *70*, 104546.
[102] Y.-W. Cai, X.-N. Zhang, G.-G. Wang, G.-Z. Li, D.-Q. Zhao, N. Sun, F. Li, H.-Y. Zhang, J.-C. Han, Y. Yang, *Nano Energy* **2021**, *81*, 105663.
[103] J. Li, Y. Liu, M. Wu, K. Yao, Z. Gao, Y. Gao, X. Huang, T. H. Wong, J. Zhou, D. Li, H. Li, J. Li, Y. Huang, R. Shi, J. Yu, X. Yu, *Fundam. Res.* **2022**, https://doi.org/10.1016/j.fmre.2022.01.021.
[104] L. Wang, Y. Liu, Q. Liu, Y. Zhu, H. Wang, Z. Xie, X. Yu, Y. Zi, *Microsyst. Nanoeng.* **2020**, *6*, 59.
[105] a) P. Ripka, *J. Phys.: Conf. Ser.* **2013**, *450*, 012001; b) J. Lenz, S. Edelstein, *IEEE Sens. J.* **2006**, *6*, 631.
[106] a) H. Emmerich, M. Schofthaler, *IEEE Trans. Electron Devices* **2000**, *47*, 972; b) H. Heidari, E. Bonizzoni, U. Gatti, F. Maloberti, R. Dahiya, *IEEE Sens. J.* **2016**, *16*, 8736.
[107] Y. Yang, L. Lin, Y. Zhang, Q. Jing, T.-C. Hou, Z. L. Wang, *ACS Nano* **2012**, *6*, 10378.
[108] S. Hajra, V. Vivekananthan, M. Sahu, G. Khandelwal, N. P. M. Joseph Raj, S.-J. Kim, *Nano Energy* **2021**, *85*, 105964.
[109] a) M. Yu, S. Qi, J. Fu, P. A. Yang, M. Zhu, *Smart Mater. Struct.* **2015**, *24*, 045009; b) W. H. Li, M. Nakano, *Smart Mater. Struct.* **2013**, *22*, 055035.
[110] a) F. H. L. Koppens, T. Mueller, P. Avouris, A. C. Ferrari, M. S. Vitiello, M. Polini, *Nat. Nanotechnol.* **2014**, *9*, 780; b) M. Peng, Z. Wen, M. Shao, X. Sun, *J. Mater. Chem. C* **2017**, *5*, 7521; c) M. Ahmadi, T. Wu, B. Hu, *Adv. Mater.* **2017**, *29*, 1605242; d) C. Chen, J. Cao, Q. Lu, X. Wang, L. Song, Z. Niu, J. Chen, *Adv. Funct. Mater.* **2017**, *27*, 1604639; e) X. Ren, Z. Li, Z. Huang, D. Sang, H. Qiao, X. Qi, J. Li, J. Zhong, H. Zhang, *Adv. Funct. Mater.* **2017**, *27*, 1606834; f) Y. Kumaresan, G. Min, A. S. Dahiya, A. Ejaz, D. Shakthivel, R. Dahiya, *Adv. Mater. Technol.* **2022**, *7*, 2100804; g) C. G. Núñez, A. Vilouras, W. T. Navaraj, F. Liu, R. Dahiya, *IEEE Sens. J.* **2018**, *18*, 7881; h) C. García Núñez, F. Liu, W. T. Navaraj, A. Christou, D. Shakthivel, R. Dahiya, *Microsyst. Nanoeng.* **2018**, *4*, 22.
[111] a) X. Li, C. Gao, H. Duan, B. Lu, X. Pan, E. Xie, *Nano Energy* **2012**, *1*, 640; b) X. Li, C. Gao, H. Duan, B. Lu, Y. Wang, L. Chen, Z. Zhang, X. Pan, E. Xie, *Small* **2013**, *9*, 2005; c) Y.-Q. Bie, Z.-M. Liao, H.-Z. Zhang, G.-R. Li, Y. Ye, Y.-B. Zhou, J. Xu, Z.-X. Qin, L. Dai, D.-P. Yu, *Adv. Mater.* **2011**, *23*, 649.
[112] a) G. Cheng, H. Zheng, F. Yang, L. Zhao, M. Zheng, J. Yang, H. Qin, Z. Du, Z. L. Wang, *Nano Energy* **2018**, *44*, 208; b) Z. Wen, J. Fu, L. Han, Y. Liu, M. Peng, L. Zheng, Y. Zhu, X. Sun, Y. Zi, *J. Mater. Chem. C* **2018**, *6*, 11893.
[113] Z.-H. Lin, G. Cheng, Y. Yang, Y. S. Zhou, S. Lee, Z. L. Wang, *Adv. Funct. Mater.* **2014**, *24*, 2810.
[114] S. D. Stranks, G. E. Eperon, G. Grancini, C. Menelaou, M. J. P. Alcocer, T. Leijtens, L. M. Herz, A. Petrozza, H. J. Snaith, *Science* **2013**, *342*, 341.
[115] L. Su, Z. Zhao, H. Li, Y. Wang, S. Kuang, G. Cao, Z. Wang, G. Zhu, *J. Mater. Chem. C* **2016**, *4*, 10395.
[116] a) A. S. M. I. Uddin, G.-S. Chung, *Sens. Actuators, B* **2017**, *245*, 1; b) F. Ejehi, R. Mohammadpour, E. Asadian, P. Sasanpour, S. Fardindoost, O. Akhavan, *Sci. Rep.* **2020**, *10*, 7312.
[117] a) K. Zhao, G. Gu, Y. Zhang, B. Zhang, F. Yang, L. Zhao, M. Zheng, G. Cheng, Z. Du, *Nano Energy* **2018**, *53*, 898; b) T. Suzuki, A. Sackmann, A. Oprea, U. Weimar, N. Bârsan, *ACS Sens.* **2020**, *5*, 2555; c) N. J. Pineau, S. D. Keller, A. T. Güntner, S. E. Pratsinis, *Microchim. Acta* **2020**, *187*, 96.
[118] a) A. S. M. Iftekhar Uddin, D.-T. Phan, G.-S. Chung, *Sens. Actuators, B* **2015**, *207*, 362; b) N. Tamaekong, C. Liewhiran, A. Wisitsoraat, S. Phanichphant, *Sens. Actuators, B* **2011**, *152*, 155; c) K. Zheng, C. Zheng, Q. He, D. Yao, L. Hu, Y. Zhang, Y. Wang, F. K. Tittel, *Opt. Express* **2018**, *26*, 26205.
[119] A. S. M. I. Uddin, U. Yaqoob, G.-S. Chung, *ACS Appl. Mater. Interfaces* **2016**, *8*, 30079.
[120] A. S. M. I. Uddin, P. S. Kumar, K. Hassan, H. C. Kim, *Sens. Actuators, B* **2018**, *258*, 857.
[121] J. Chang, H. Meng, C. Li, J. Gao, S. Chen, Q. Hu, H. Li, L. Feng, *Adv. Mater. Technol.* **2020**, *5*, 1901087.
[122] S.-H. Shin, Y. H. Kwon, Y.-H. Kim, J.-Y. Jung, J. Nah, *Nanomaterials* **2016**, *6*, 186.
[123] a) Y.-H. Zhang, C.-N. Wang, F.-L. Gong, P. Wang, U. Guharoy, C. Yang, H.-L. Zhang, S.-M. Fang, J. Liu, *J. Hazard. Mater.* **2020**, *388*, 122069; b) Y. Lv, H. Yu, P. Xu, J. Xu, X. Li, *Sens. Actuators, B* **2018**, *256*, 639.
[124] S.-J. Kim, S.-J. Choi, J.-S. Jang, H.-J. Cho, W.-T. Koo, H. L. Tuller, I.-D. Kim, *Adv. Mater.* **2017**, *29*, 1700737.
[125] a) M. Z. Jacobson, W. G. Colella, D. M. Golden, *Science* **2005**, *308*, 1901; b) R. F. Service, *Science* **2004**, *305*, 958; c) T. Hübert,

L. Boon-Brett, G. Black, U. Banach, *Sens. Actuators, B* **2011**, *157*, 329; d) M. G. Chung, D.-H. Kim, D. K. Seo, T. Kim, H. U. Im, H. M. Lee, J.-B. Yoo, S.-H. Hong, T. J. Kang, Y. H. Kim, *Sens. Actuators, B* **2012**, *169*, 387.
[126] A. S. M. I. Uddin, G.-S. Chung, *Sens. Actuators, B* **2016**, *231*, 601.
[127] a) R. Khan, H. W. Ra, J. T. Kim, W. S. Jang, D. Sharma, Y. H. Im, *Sens. Actuators, B* **2010**, *150*, 389; b) W. J. Park, K. J. Choi, M. H. Kim, B. H. Koo, J.-L. Lee, J. M. Baik, *ACS Appl. Mater. Interfaces* **2013**, *5*, 6802.
[128] A. S. M. I. Uddin, G.-S. Chung, *RSC Adv.* **2016**, *6*, 63030.
[129] S. Cui, Y. Zheng, T. Zhang, D. Wang, F. Zhou, W. Liu, *Nano Energy* **2018**, *49*, 31.
[130] a) J. Lelieveld, J. S. Evans, M. Fnais, D. Giannadaki, A. Pozzer, *Nature* **2015**, *525*, 367; b) M. Jerrett, *Nature* **2015**, *525*, 330; c) D. K. Bandgar, S. T. Navale, S. R. Nalage, R. S. Mane, F. J. Stadler, D. K. Aswal, S. K. Gupta, V. B. Patil, *J. Mater. Chem. C* **2015**, *3*, 9461; d) F. F. Franco, L. Manjakkal, D. Shakthivel, R. Dahiya, in *2019 IEEE Sensors*, IEEE, Piscataway, NJ, USA **2019**, https://doi.org/10.1109/SENSORS43011.2019.8956763.
[131] a) A. T. Güntner, M. Righettoni, S. E. Pratsinis, *Sens. Actuators, B* **2016**, *223*, 266; b) S. DuBois, S. Eng, R. Bhattacharya, S. Rulyak, T. Hubbard, D. Putnam, D. J. Kearney, *Dig. Dis. Sci.* **2005**, *50*, 1780.
[132] H. Wang, S. I. Vagin, B. Rieger, A. Meldrum, *ACS Appl. Mater. Interfaces* **2020**, *12*, 20507.
[133] H. Wang, H. Wu, D. Hasan, T. He, Q. Shi, C. Lee, *ACS Nano* **2017**, *11*, 10337.
[134] a) A. Sharma, M. Tomar, V. Gupta, *Sens. Actuators, B* **2013**, *181*, 735; b) R. Ehrlich, M. C. Henry, *Arch. Env. Health: Int. J.* **1968**, *17*, 860; c) K. Mukala, J. Pekkanen, P. Tiittanen, S. Alm, R. Salonen, J. Tuomisto, *Eur. Respir. J.* **1999**, *13*, 1411; d) G. Sberveglieri, P. Benussi, G. Coccoli, S. Groppelli, P. Nelli, *Thin Solid Films* **1990**, *186*, 349.
[135] a) P. Ivanov, E. Llobet, X. Vilanova, J. Brezmes, J. Hubalek, X. Correig, *Sens. Actuators, B* **2004**, *99*, 201; b) F. Hernández-Ramírez, A. Tarancón, O. Casals, J. Arbiol, A. Romano-Rodríguez, J. R. Morante, *Sens. Actuators, B* **2007**, *121*, 3.
[136] H. S. Hong, N. H. Ha, D. D. Thinh, N. H. Nam, N. T. Huong, N. Thi Hue, T. V. Hoang, *Nano Energy* **2021**, *87*, 106165.
[137] a) X. Fang, B. Zong, S. Mao, *Nano-Micro Lett.* **2018**, *10*, 64; b) T. Zhong, H. Guan, Y. Dai, H. He, L. Xing, Y. Zhang, X. Xue, *Nano Energy* **2019**, *60*, 52; c) D. Zhang, J. Liu, C. Jiang, A. Liu, B. Xia, *Sens. Actuators, B* **2017**, *240*, 55.
[138] H. He, M. Zhang, T. Zhao, H. Zeng, L. Xing, X. Xue, *Sci. China Mater.* **2019**, *62*, 1433.
[139] F. I. Khan, A. Kr , Ghoshal, *J. Loss Prevention Process Ind.* **2000**, *13*, 527.
[140] Z. Wen, L. Zhu, W. Mei, Y. Li, L. Hu, L. Sun, W. Wan, Z. Ye, *J. Mater. Chem. A* **2013**, *1*, 7511.
[141] H. Nguyen, S. A. El-Safty, *J. Phys. Chem. C* **2011**, *115*, 8466.
[142] Z. Ren, Y. Ding, J. Nie, F. Wang, L. Xu, S. Lin, X. Chen, Z. L. Wang, *ACS Appl. Mater. Interfaces* **2019**, *11*, 6143.
[143] a) C. Deng, J. Zhang, X. Yu, W. Zhang, X. Zhang, *J. Chromatogr. B* **2004**, *810*, 269; b) Y. S. Kim, S.-C. Ha, H. Yang, Y. T. Kim, *Sens. Actuators, B* **2007**, *122*, 211; c) H. Ahn, Y. Wang, S. H. Jee, M. Park, Y. S. Yoon, D.-J. Kim, *Chem. Phys. Lett.* **2011**, *511*, 331.
[144] Y. Su, T. Yang, X. Zhao, Z. Cai, G. Chen, M. Yao, K. Chen, M. Bick, J. Wang, S. Li, G. Xie, H. Tai, X. Du, Y. Jiang, J. Chen, *Nano Energy* **2020**, *74*, 104941.
[145] B. Liu, S. Wang, Z. Yuan, Z. Duan, Q. Zhao, Y. Zhang, Y. Su, Y. Jiang, G. Xie, H. Tai, *Nano Energy* **2020**, *78*, 105256.
[146] G. Khandelwal, A. Chandrasekhar, R. Pandey, N. P. Maria Joseph Raj, S.-J. Kim, *Sens. Actuators, B* **2019**, *282*, 590.
[147] J.-H. Kim, J. Chun, J. W. Kim, W. J. Choi, J. M. Baik, *Adv. Funct. Mater.* **2015**, *25*, 7049.
[148] a) J. Zhou, S. Dag, S. D. Senanayake, B. C. Hathorn, S. V. Kalinin, V. Meunier, D. R. Mullins, S. H. Overbury, A. P. Baddorf, *Phys. Rev. B* **2006**, *74*, 125318; b) M. Nagao, Y. Suda, *Langmuir* **1989**, *5*, 42.
[149] a) T. W. Clarkson, L. Magos, G. J. Myers, *N. Engl. J. Med.* **2003**, *349*, 1731; b) F. Zahir, S. J. Rizwi, S. K. Haq, R. H. Khan, *Environ. Toxicol. Pharmacol.* **2005**, *20*, 351.
[150] a) F. Fu, Q. Wang, *J. Env. Manage.* **2011**, *92*, 407; b) E. S. Forzani, H. Zhang, W. Chen, N. Tao, *Environ. Sci. Technol.* **2005**, *39*, 1257.
[151] D. C. Evers, S. E. Keane, N. Basu, D. Buck, *Sci. Total Environ.* **2016**, *569*, 888.
[152] a) J.-S. Lee, M. S. Han, C. A. Mirkin, *Angew. Chem., Int. Ed.* **2007**, *46*, 4093; b) J. Liu, Y. Lu, *Angew. Chem., Int. Ed.* **2007**, *46*, 7587; c) D. Li, A. Wieckowska, I. Willner, *Angew. Chem., Int. Ed.* **2008**, *47*, 3927; d) T. Senapati, D. Senapati, A. K. Singh, Z. Fan, R. Kanchanapally, P. C. Ray, *Chem. Commun.* **2011**, *47*, 10326; e) D. Wen, L. Deng, S. Guo, S. Dong, *Anal. Chem.* **2011**, *83*, 3968.
[153] Z.-H. Lin, G. Zhu, Y. S. Zhou, Y. Yang, P. Bai, J. Chen, Z. L. Wang, *Angew. Chem., Int. Ed.* **2013**, *52*, 5065.
[154] Z. Li, J. Chen, H. Guo, X. Fan, Z. Wen, M.-H. Yeh, C. Yu, X. Cao, Z. L. Wang, *Adv. Mater.* **2016**, *28*, 2983.
[155] M. A. Warner, J. V. Harper, *Anesthesiology* **1985**, *62*, 366.
[156] a) T. Zhao, J. He, X. Wang, B. Ma, X. Wang, L. Zhang, P. Li, N. Liu, J. Lu, X. Zhang, *J. Pharm. Biomed. Anal.* **2014**, *98*, 311; b) X. X. Han, L. Chen, U. Kuhlmann, C. Schulz, I. M. Weidinger, P. Hildebrandt, *Angew. Chem., Int. Ed.* **2014**, *53*, 2481; c) H. Li, Y. Chen, Y. Zhang, W. Han, X. Sun, J. Li, L. Wang, *J. Electroanal. Chem.* **2013**, *689*, 193.
[157] D. Cinghită, C. Radovan, D. Dascălu, *Sensors* **2008**, *8*, 4560.
[158] P. Schyman, R. L. Printz, S. K. Estes, K. L. Boyd, M. Shiota, A. Wallqvist, *Front. Pharmacol.* **2018**, *9*, 1272.
[159] M. A. Kafi, A. Paul, A. Vilouras, R. Dahiya, *Biosens. Bioelectron.* **2020**, *147*, 111781.
[160] a) P. E. M. Phillips, G. D. Stuber, M. L. A. V. Heien, R. M. Wightman, R. M. Carelli, *Nature* **2003**, *422*, 614; b) M. W. Howe, P. L. Tierney, S. G. Sandberg, P. E. M. Phillips, A. M. Graybiel, *Nature* **2013**, *500*, 575; c) T. Lee, L. X. Cai, V. S. Lelyveld, A. Hai, A. Jasanoff, *Science* **2014**, *344*, 533; d) M. B. Santana, P. Halje, H. Simplício, U. Richter, M. Aurelio, M. Freire, P. Petersson, R. Fuentes, M. A. L. Nicolelis, *Neuron* **2014**, *84*, 716; e) C. R. Schubert, H. S. Xi, J. R. Wendland, P. O'Donnell, *Neuron* **2014**, *84*, 537; f) S. Lammel, E. E. Steinberg, C. Földy, N. R. Wall, K. Beier, L. Luo, R. C. Malenka, *Neuron* **2015**, *85*, 429.
[161] a) J. J. VanDersarl, A. Mercanzini, P. Renaud, *Adv. Funct. Mater.* **2015**, *25*, 78; b) M. Zhang, C. Liao, Y. Yao, Z. Liu, F. Gong, F. Yan, *Adv. Funct. Mater.* **2014**, *24*, 1036; c) B.-R. Li, Y.-J. Hsieh, Y.-X. Chen, Y.-T. Chung, C.-Y. Pan, Y.-T. Chen, *J. Am. Chem. Soc.* **2013**, *135*, 16034; d) H. Y. Yue, S. Huang, J. Chang, C. Heo, F. Yao, S. Adhikari, F. Gunes, L. C. Liu, T. H. Lee, E. S. Oh, B. Li, J. J. Zhang, T. Q. Huy, N. V. Luan, Y. H. Lee, *ACS Nano* **2014**, *8*, 1639.
[162] J. Weng, J. Xue, J. Wang, J. Ye, H. Cui, F. Sheu, Q. Zhang, *Adv. Funct. Mater.* **2005**, *15*, 639.
[163] S. Hong, Y. S. Na, S. Choi, I. T. Song, W. Y. Kim, H. Lee, *Adv. Funct. Mater.* **2012**, *22*, 4711.
[164] X.-G. Wang, J. Li, Y.-J. Fan, *Microchim. Acta* **2010**, *169*, 173.
[165] Z.-H. Lin, Y. Xie, Y. Yang, S. Wang, G. Zhu, Z. L. Wang, *ACS Nano* **2013**, *7*, 4554.
[166] a) J. Hu, P.-C. Zheng, J.-H. Jiang, G.-L. Shen, R.-Q. Yu, G.-K. Liu, *Anal. Chem.* **2009**, *81*, 87; b) M. L. Nierodzik, S. Karpatkin, *Cancer Cell* **2006**, *10*, 355.
[167] M. A. Shuman, P. W. Majerus, *J. Clin. Invest.* **1976**, *58*, 1249.
[168] B. Deng, Y. Lin, C. Wang, F. Li, Z. Wang, H. Zhang, X.-F. Li, X. C. Le, *Anal. Chim. Acta* **2014**, *837*, 1.
[169] S. D. Jayasena, *Clin. Chem.* **1999**, *45*, 1628.
[170] a) B. Gao, Y. Li, Z. Zhang, *J. Chromatogr. B* **2010**, *878*, 2077; b) B. Khadro, C. Sanglar, A. Bonhomme, A. Errachid, N. Jaffrezic-Renault, *Proc. Eng.* **2010**, *5*, 371; c) S. Narayanan, H. D. Appleton,

Clin. Chem. **1980**, *26*, 1119; d) J. Coresh, B. C. Astor, T. Greene, G. Eknoyan, A. S. Levey, *Am. J. Kidney Dis.* **2003**, *41*, 1; e) E. Mohabbati-Kalejahi, V. Azimirad, M. Bahrami, A. Ganbari, *Talanta* **2012**, *97*, 1.

[171] a) R. C. Miller, E. Brindle, D. J. Holman, J. Shofer, N. A. Klein, M. R. Soules, K. A. O'Connor, *Clin. Chem.* **2004**, *50*, 924; b) E. D. Moreira, R. C. S. Neves, Z. O. Nunes, M. C. C. de Almeida, A. B. V. Mendes, J. A. S. Fittipaldi, F. Ablan, *Diabetes Res. Clin. Pract.* **2010**, *87*, 407.

[172] a) T. Lee, J. Lim, K. Park, E.-K. Lim, J.-J. Lee, *ACS Sens.* **2020**, *5*, 3099; b) X. Lin, X. Huang, Y. Zhu, K. Urmann, X. Xie, M. R. Hoffmann, *ACS Nano* **2018**, *12*, 10281.

[173] a) M. D. Disney, J. Zheng, T. M. Swager, P. H. Seeberger, *J. Am. Chem. Soc.* **2004**, *126*, 13343; b) S. Tok, K. de Haan, D. Tseng, C. F. Usanmaz, H. Ceylan Koydemir, A. Ozcan, *Lab Chip* **2019**, *19*, 2925; c) J. Lee, I. S. Kim, H.-W. Yu, *Anal. Chem.* **2010**, *82*, 2836; d) L. Yang, R. Bashir, *Biotechnol. Adv.* **2008**, *26*, 135; e) D. Ivnitski, I. Abdel-Hamid, P. Atanasov, E. Wilkins, *Biosens. Bioelectron.* **1999**, *14*, 599.

[174] a) H. Gao, J. M. Korn, S. Ferretti, J. E. Monahan, Y. Wang, M. Singh, C. Zhang, C. Schnell, G. Yang, Y. Zhang, O. A. Balbin, S. Barbe, H. Cai, F. Casey, S. Chatterjee, D. Y. Chiang, S. Chuai, S. M. Cogan, S. D. Collins, E. Dammassa, N. Ebel, M. Embry, J. Green, A. Kauffmann, C. Kowal, R. J. Leary, J. Lehar, Y. Liang, A. Loo, E. Lorenzana, et al., *Nat. Med.* **2015**, *21*, 1318; b) P. M. Eimon, M. Ghannad-Rezaie, G. De Rienzo, A. Allalou, Y. Wu, M. Gao, A. Roy, J. Skolnick, M. F. Yanik, *Nat. Commun.* **2018**, *9*, 219.

[175] a) N. Cermak, S. Olcum, F. F. Delgado, S. C. Wasserman, K. R. Payer, M. A. Murakami, S. M. Knudsen, R. J. Kimmerling, M. M. Stevens, Y. Kikuchi, A. Sandikci, M. Ogawa, V. Agache, F. Baléras, D. M. Weinstock, S. R. Manalis, *Nat. Biotechnol.* **2016**, *34*, 1052; b) Q. Chen, Z. He, W. Liu, X. Lin, J. Wu, H. Li, J.-M. Lin, *Adv. Healthcare Mater.* **2015**, *4*, 2291.

[176] S. M. Jakob, E. Ruokonen, J. Takala, *Shock* **2002**, *18*, 8.

[177] O. Hamzaoui, J.-F. Georger, X. Monnet, H. Ksouri, J. Maizel, C. Richard, J.-L. Teboul, *Crit. Care* **2010**, *14*, R142.

[178] G. D. Perkins, C. Ji, C. D. Deakin, T. Quinn, J. P. Nolan, C. Scomparin, S. Regan, J. Long, A. Slowther, H. Pocock, J. J. M. Black, F. Moore, R. T. Fothergill, N. Rees, L. O'shea, M. Docherty, I. Gunson, K. Han, K. Charlton, J. Finn, S. Petrou, N. Stallard, S. Gates, R. Lall, *N. Engl. J. Med.* **2018**, *379*, 711.

[179] V. J. J. Cadete, J. Sawicka, D. Polewicz, A. Doroszko, M. Wozniak, G. Sawicki, *Proteomics* **2010**, *10*, 4377.

[180] B. Guldiken, J. Rémi, S. Noachtar, *J. Neurol.* **2016**, *263*, 861.

[181] C. Sirois, J. Couture, J.-P. Grégoire, *Ther. Adv. Drug Saf.* **2012**, *3*, 213.

[182] P. Ma, T. Li, F. Ji, H. Wang, J. Pang, *Int. J. Clin. Exp. Med.* **2015**, *8*, 14296.

[183] M. Natarajan Savitha, S. Sarkar, K. N. Suvilesh, S. L. Shravan Kumar, B. S. Vishwanath, *Prog. Biol.* **2019**, *3*, 20.

[184] S. M. Lee, M. Hutchinson, V. Staikopoulos, D. A. Saint, *Int. J. Cardiol.* **2015**, *190*, 353.

[185] U. C. Dubach, B. Rosner, T. Stürmer, *N. Engl. J. Med.* **1991**, *324*, 155.

[186] X. Liu, D. Huang, C. Lai, G. Zeng, L. Qin, C. Zhang, H. Yi, B. Li, R. Deng, S. Liu, Y. Zhang, *TrAC Trends Anal. Chem.* **2018**, *109*, 260.

[187] a) R. T. Kushikawa, M. R. Silva, A. C. D. Angelo, M. F. S. Teixeira, *Sens. Actuators, B* **2016**, *228*, 207; b) D. Huang, W. Xue, G. Zeng, J. Wan, G. Chen, C. Huang, C. Zhang, M. Cheng, P. Xu, *Water Res.* **2016**, *106*, 15.

[188] D. F. Williams, *Biomaterials* **2014**, *35*, 10009.

[189] T. Korzinskas, O. Jung, R. Smeets, S. Stojanovic, S. Najman, K. Glenske, M. Hahn, S. Wenisch, R. Schnettler, M. Barbeck, *Int. J. Mol. Sci.* **2018**, *19*, 2952.

[190] S. Chen, X. Fan, C. Zhang, A. Wei, W. Chen, *Mater. Sci. Eng., C* **2021**, *126*, 112118.

[191] B. B. Karakoçak, R. Raliya, J. T. Davis, S. Chavalmane, W.-N. Wang, N. Ravi, P. Biswas, *Toxicol. In Vitro* **2016**, *37*, 61.

[192] M. C. Bélanger, Y. Marois, *J. Biomed. Mater. Res.* **2001**, *58*, 467.

[193] G. Khandelwal, N. P. Maria Joseph Raj, S.-J. Kim, *Adv. Energy Mater.* **2021**, *11*, 2101170.

[194] B. Stadlober, M. Zirkl, M. Irimia-Vladu, *Chem. Soc. Rev.* **2019**, *48*, 1787.

[195] a) S. Donati, *Meas. Sci. Technol.* **2001**, *12*, 653; b) J. Chen, W. Ouyang, W. Yang, J.-H. He, X. Fang, *Adv. Funct. Mater.* **2020**, *30*, 1909909; c) Z. Wu, T. Cheng, Z. L. Wang, *Sensors* **2020**, *20*, 2925.

[196] a) S. Kim, P. Eichhorn, J. N. Jensen, A. S. Weber, D. S. Aga, *Environ. Sci. Technol.* **2005**, *39*, 5816; b) M. B. Gumpu, S. Sethuraman, U. M. Krishnan, J. B. B. Rayappan, *Sens. Actuators, B* **2015**, *213*, 515.

[197] a) M. C. Turner, Z. J. Andersen, A. Baccarelli, W. R. Diver, S. M. Gapstur, C. A. PopeIII, D. Prada, J. Samet, G. Thurston, A. Cohen, *Ca-Cancer J. Clin.* **2020**, *70*, 460; b) World Health Organization, 9 out of 10 people worldwide breathe polluted air, but more countries are taking action, https://www.who.int/news/item/02-05-2018-9-out-of-10-people-worldwide-breathe-polluted-air-but-more-countries-are-taking-action (accessed: January 2022).

[198] J. W. Lee, S. Jung, T. W. Lee, J. Jo, H. Y. Chae, K. Choi, J. J. Kim, J. H. Lee, C. Yang, J. M. Baik, *Adv. Energy Mater.* **2019**, *9*, 1901987.

[199] R. Huerta, T. Mosqueiro, J. Fonollosa, N. F. Rulkov, I. Rodriguez-Lujan, *Chemom. Intell. Lab. Syst.* **2016**, *157*, 169.

[200] S. Pan, Z. Zhang, *Friction* **2019**, *7*, 2.

[201] a) C. K. Chung, K. H. Ke, *Appl. Surf. Sci.* **2020**, *508*, 145310; b) G. Min, Y. Xu, P. Cochran, N. Gadegaard, D. M. Mulvihill, R. Dahiya, *Nano Energy* **2021**, *83*, 105829.

[202] W. Yang, X. Wang, H. Li, J. Wu, Y. Hu, Z. Li, H. Liu, *Nano Energy* **2019**, *57*, 41.

[203] a) G. Khandelwal, N. P. Maria Joseph Raj, S.-J. Kim, *J. Mater. Chem. A* **2020**, *8*, 17817; b) Y. Zhang, J. Wu, S. Cui, W. Wei, W. Chen, R. Pang, Z. Wu, L. Mi, *Chem. – Eur. J.* **2020**, *26*, 584.

[204] M. Y. Han, B. Özyilmaz, Y. Zhang, P. Kim, *Phys. Rev. Lett.* **2007**, *98*, 206805.

[205] A. Ryzhikov, M. Labeau, A. Gaskov, in *Conf. Proc. Sensors for Environment, Health and Security*, (Ed: M.-I. Baraton) Springer, Dordrecht, The Netherlands **2009**, pp. 141–157.

[206] Y. Dong, S. S. K. Mallineni, K. Maleski, H. Behlow, V. N. Mochalin, A. M. Rao, Y. Gogotsi, R. Podila, *Nano Energy* **2018**, *44*, 103.

[207] Aaryashree, S. S. , P. Walke, S. K. Nayak, C. S. Rout, D. J. Late, *Nano Res.* **2021**, *14*, 3669.

[208] N. Saadati, M. P. Abdullah, Z. Zakaria, S. B. T. Sany, M. Rezayi, H. Hassonizadeh, *Chem. Cent. J.* **2013**, *7*, 63.

[209] B. D. Chen, W. Tang, C. He, T. Jiang, L. Xu, L. P. Zhu, G. Q. Gu, J. Chen, J. J. Shao, J. J. Luo, Z. L. Wang, *Adv. Mater. Technol.* **2018**, *3*, 1700229.

[210] L. D. Tijing, Y. C. Woo, J.-S. Choi, S. Lee, S.-H. Kim, H. K. Shon, *J. Membr. Sci.* **2015**, *475*, 215.

[211] X. Wang, Z. Wen, H. Guo, C. Wu, X. He, L. Lin, X. Cao, Z. L. Wang, *ACS Nano* **2016**, *10*, 11369.

[212] a) Y. Chen, Y. Zhang, T. Zhan, Z. Lin, S. L. Zhang, H. Zou, G. Zhang, C. Zou, Z. L. Wang, *Adv. Mater. Technol.* **2019**, *4*, 1900075; b) Y. Liu, C. Hu, *Nanoscale* **2020**, *12*, 20118.

[213] J. Wu, Y. Xi, Y. Shi, *Nano Energy* **2020**, *72*, 104659.

[214] a) A. Christou, F. Liu, R. Dahiya, *Microsyst. Nanoeng.* **2021**, *7*, 82; b) A. Zumeit, A. S. Dahiya, A. Christou, D. Shakthivel, R. Dahiya, *npj Flexible Electron.* **2021**, *5*, 18.

Gaurav Khandelwal is currently working as a post-doctoral fellow in the Bendable Electronics and Sensing Technologies (BEST) research group at the University of Glasgow. He completed his Ph.D. (with excellence) from the Department of Mechatronics Engineering at Jeju National University, South Korea, where he received the Brain Korea fellowship. He holds a Bachelor's and Master's degree in Nanotechnology from the Centre for Converging Technologies, U.O.R, India. He worked as Project Associate at the Indian Institute of Technology (IIT), Delhi, India. He also worked as a research intern in the field of peptide-based nanofibers at the Institute of Nano Science and Technology (INST), India. His current research area includes triboelectric nanogenerators, piezoelectric nanogenerators, self-powered sensors, and nanomaterial synthesis and characterization.

Ravinder Dahiya is professor of electronics and nanoengineering at the University of Glasgow, UK. He is the leader of the Bendable Electronics and Sensing Technologies (BEST) research group, which conducts fundamental and applied research in flexible and printed electronics, tactile sensing, electronic skin, robotics, and wearable systems. He has authored or co-authored more than 400 publications, books and submitted/granted patents and disclosures. He is President (2022–2023) of IEEE Sensors Council and the Founding Editor-in-Chief of IEEE Journal on Flexible Electronics (J-FLEX). He has received several awards, including Technical Achievement award from IEEE Sensors Council, Young Investigator Award from Elsevier, and 11 best journal/conference paper awards as author/co-author. He is a Fellow of the IEEE and the Royal Society of Edinburgh.